MONTE CARLO SIMULATIONS OF COMPLEX GERMANIUM ESCAPE SUPPRESSION SPECTROMETERS WITH MCNPX

A CASE STUDY

Andrew John Esau

Thesis presented in fulfillment of the requirements for the degree of

Magister Scientiae at the University of Western Cape

Supervisor: Prof. R Lindsay

Department of Physics

University of the Western Cape

Co-supervisor: Mr. PP Maleka

Department of Physics

University of the Western Cape

June 2009

UNIVERSITY of the
WESTERN CAPE

DECLARATION

I, the undersigned, hereby declare that the work contained in this thesis is my own original work and that I have not previously in its entirety or in part submitted it at any university for a degree.

Signature: ……

Date: ……

UNIVERSITY of the
WESTERN CAPE

ABSTRACT

MONTE CARLO SIMULATIONS OF COMPLEX GERMANIUM ESCAPE SUPPRESSION SPECTROMETERS WITH MCNPX: A CASE STUDY

Andrew John Esau

Gamma ray spectroscopy has provided enormous amounts of information on the behaviour and structure of atomic nuclei [SHA88, BEA92, EBE08]. Most of the major discoveries in experimental nuclear physics over the last five decades are strongly associated with improvements in detector technologies. Inorganic scintilators led to the discovery in 1963 of the first excited states of a rotational band based on the ground state of ^{162}Dy. Improvements in peak-to-background ratios and detector resolutions obtained with germanium led to the first evidence of backbending which is associated with a two quasi-particle excitation in ^{162}Dy [SHA88]. More recently the development of composite and highly-segmented Ge detectors has significantly increased the performance and power of detection systems.

The Clover detector is such a detector system and is in use at iThemba LABS. This study concerns the evaluation of the particle transport code MCNPX 2.5.0 as a tool to model complex composite detectors such as the Clover. Lanthanum silicate (LSO) and Lead tungstate (PbWO) are also evaluated as possible suppressor shield materials.

It is shown that reasonable agreement between experiment and simulation is found when the experiment is accurately reproduced. However, when complex detection modes are implemented in the detector based on the number of elements that fire, MCNPX cannot be used to model the detector performance exactly. Differences between simulated and experimental results are found in suppressed add-back mode. It is proposed that the discrepancies are due to limitations in implementation of the pulse-height and special anti-coincidence tally in MCNPX.

LSO and PbWO are compared to BGO as suppressor shield materials. It is found that LSO is not an ideal material for a suppression shield. PbWO is shown to give

performance values similar to that of BGO. The back-plug is shown to have no effect on the Peak-to-Total ratio but is effective at reducing the background at lower energies.

DEDICATION

To:

1. The memory of my late grandfather Andries Philander, who while being illiterate and a lowly sheepshearer, and eventually a successful small scale sheep farmer who believed in the value of a good education.

2. To my girlfriend Morina Rondia Norton, who has been with me since we met about 15 years ago. I have been honored to have you by my side every step of the way. You really are a masterpiece of nature.

ACKNOWLEDGEMENTS

I am greatly indebted to the following people who made this thesis possible:

- Prof. Robbie Lindsay, supervisor, for his guidance, active involvement, support and financial contribution in the preparation of this study.

- Mr. Peane Maleka co-supervisor, who was with me every step of this study, for his valuable suggestions, guidance, and technical support throughout this project.

- NRF, for their financial support throughout this research.

- Dr. E Lawrie and Dr D Roux, who, with no benefit to themselves, helped me to set-up the experiment and were kind enough to help me with the software and data collection at Ithemba.

- Dr JJ Lawrie, who was always available to assist with information regarding the Clover detector at Ithemba and its operation as well as answering all my questions in a timeous fashion, and giving me some of his own results that are cited in this thesis.

- Dr R Bark who kept me informed about the opening of a Clover detector at Ithemba.

- Prof J.F Sharpey-Schaefer who proposed the study that led to this thesis, without whom, this thesis would not have happened.

- To my friends; Mr J Fielies (Herby), my oldest friend with whom I literally grew up and his wife, Mrs E Fielies, who were always ready to provide sustenance on my many unannounced visits. Mr A Lewak and wife S Lewak for same and making sure that when things got stressful, a party was to be had. Mr D Du Plessis for always being ready to take me to a party and reminding

me life is not all work, but can actually be lots ‘a play as well. Throughout my undergrad and post-grad studies he was always at the ready to provide housing in Gauteng when my studies demanded it. To all the other not mentioned (the list will become too long!) here, you were and still are all great. Thank you for being the best human beings a person can hope to meet

- To my fellow students and friends, En Zhou, Thobeka Wittes, Tshepo Dinoko, Takalani Madima and Aron Maibi Malape for their moral support and assistance throughout my studies.

- To Dr Mojafela Moeketsi (Daniel), for always being ready for a discussion of physics, mathematics and everything else and for teaching me that physics is a mathematical formulation that requires a physical explanation.

- To my parents Mr H Esau and Mrs M Esau for just being great parents and good people, brothers Mr S Philander and Mr HJ Esau, sisters, Mrs E van Rensburg and Ms K Philander who kept house for me all these years and the youngest of us all, my little sister, Ms AJ Esau for always being supportive and being on my side whenever I needed them.

- UWC Physics Department, in particular Mrs. Angela Adams for their warm welcome and making me feel at home, and for their encouragement and kind support.

UNIVERSITY of the
WESTERN CAPE

CONTENTS

LIST OF FIGURES AND TABLES

CHAPTER 1 INTRODUCTION

It is well-known today that unstable or radioactive nuclei decay via one of three processes, namely, alpha (α), beta (β) or gamma (γ) decay to a stable nucleus. Most naturally occurring and artificially produced nuclei decay by α or β decay to stable nuclei [LIL01]. Heavy nuclei ($82 < Z \leq 92$) will most likely decay via alpha decay as the emission of this heavy particle is accompanied by significant energy loss, while neutron rich or proton rich nuclei decay through positive or negative beta decay towards the stability line.

A significant number of nuclei that decay via alpha or beta mechanisms leave the final nucleus in an excited final state. This excited nucleus decays quickly to a ground state through the emission of one or more gamma rays.

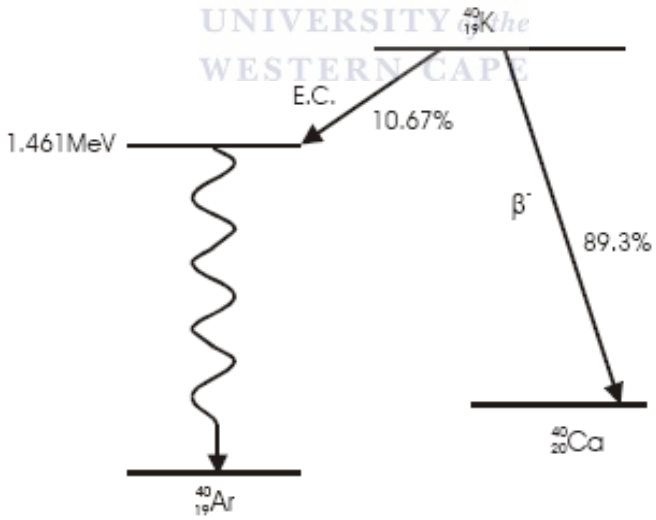

Figure 1-1: ^{40}K undergoes β decay leading to γ decay [HEN03]

Gamma-ray sources in the laboratory are usually nuclei that undergo a form of beta decay in the parent nucleus which cause the formation of a daughter nucleus that will emit the gamma-ray (Figure 1-1). The half-life of the parent nucleus that undergoes the beta decay is usually long (a matter of days or more) whilst the daughter product

has a very short half-life [KNO01]. In Figure 1-1 a daughter is formed through capture of an electron, after which the daughter emits the gamma-ray and decays to ^{40}Ar. The energy of the emitted gamma ray is the difference between the energies of the initial and final state of the parent nucleus. Electron capture - when the nucleus captures an electron - is a competing process of positive beta decay, with a similar outcome.

A significant amount of knowledge about the structure of the nucleus is experimentally obtained by gamma spectroscopy [KRA88, KNO01]. This is a consequence of the fact that it is relatively easy to observe gamma rays, and its energy can be measured with accuracy. In addition, studying the competing process to gamma-decay, namely, internal conversion- the emission of an orbital electron by an excited nucleus- makes it possible to assign spin and parity to energy levels of a nucleus [LIL01, KNO01].

The important mechanisms by which a γ-ray interacts with material are Photoelectric Effect, Compton Scattering, Pair Production and Elastic or Thomson Scattering [KRA88, KNO01].

1.1 Interaction of gamma-rays with matter

1.1.1 Photo-electric effect (PE)

In this process the gamma ray interacts with an atom, is fully absorbed by the atom, causing the ejection of an electron commonly known as a photo-electron or recoil-electron. The ejected electron is initially a bound or atomic electron of the target atom. This process can be visualized as an interaction between the photon and the whole atom, since energy and momentum cannot otherwise both be conserved. Below (Figure 1-2) is an illustration of this process.

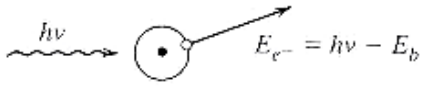

Figure 1-2 Incident photon undergoes PE [KNO01]

The photo-electron is ejected with energy E_e, where $h\nu$ is the energy of the incident photon and E_b is the binding energy of the ejected electron (Figure 1-2). The probability of this process taking place is approximated by $\tau \cong k \times \frac{Z^n}{E_\gamma^{3.5}}$, with $n \sim 3\text{-}4$ [KNO01]. This means that gamma-rays attenuate faster in materials with high Z. This has implications for detector design, in that, to ensure a high probability of interaction of gamma-rays with detector material, the material should preferably have high Z. In addition, photons with low energy are also more likely to undergo PE.

1.1.2 Compton Scattering (CS)

As illustrated in Figure 1-3 below, a photon, with energy $E = h\nu$ incident on a target is scattered, by a free or orbital electron. The incident photon is scattered with final energy E' and the electron with kinetic energy E_e.

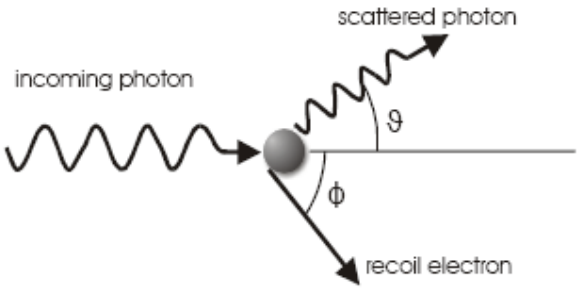

Figure 1-3 Illustration of Compton scattering [HEN03]

It can be shown, using conservation of momentum and energy principles that

$$\frac{1}{E^{'}} - \frac{1}{E} = \frac{1}{511}\left(1 - Cos\vartheta\right), \qquad (1.1)$$

where both the incident and scattered γ ray energy E, E' and the electron rest mass $m_o c^2$ = 511 are all in keV. The scattered photon has energy in the range E (see equation 1.1), for forward scattering at (a grazing) angle 0°, to a minimum of roughly 250 keV, when scattered through 180°, and the incident photon has a large energy, E. This is easily seen from an examination of equation (1.1). The cross-section for this process can be approximated by $\frac{1}{E}$ [LIL01]. As the incident gamma-ray energy increases the probability of Compton scattering becomes less-likely as can be seen in Figure 1-5.

The probability that a particle will scatter in a direction θ when undergoing CS is given by the quantum mechanical formula of Klein-Nishina [KNO01, SHA88]

$$\frac{d\sigma(\theta)}{d\Omega} = \frac{1}{2} r_0^{\,2} \left(\frac{E^{'}}{E}\right)^2 \left\{\frac{E}{E'} + \frac{E^{'}}{E} - \sin^2\theta\right\}, \qquad (1.2)$$

where

$$r_o = \frac{e^2}{4\pi\varepsilon_o mc^2} = 2.82\,fm\,. \qquad (1.3)$$

Examination of equation 1.2 shows that the angular distribution of the scattered particles becomes more dominant in the forward direction as the γ-ray energy increases as shown in Figure 1-4.

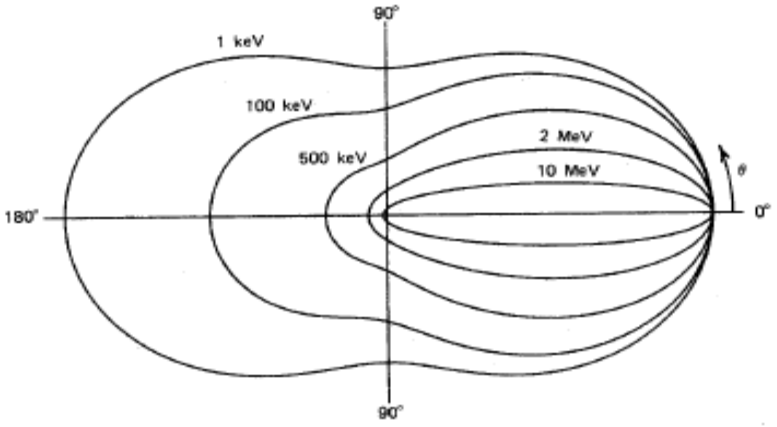

Figure 1-4 Angular distribution of scattered particles as a function of incident energy [KNO01]

1.1.3 Pair Production (PP)

Upon interaction of the photon with the atom, a positron (positive electron) and electron, the so-called positron pair is produced. The positron will eventually annihilate with an electron when its kinetic energy becomes very low and two secondary photons are emitted. The probability of this interaction occurring is approximated by $k \times Z \times E^2$ [HEN03], where k is the constant associated with PP.

This mechanism only occurs if the incident gamma energy equals at least 2 times 511 keV, which is 1.022 MeV, or exceeds it. It is the dominant process for incident γ-ray energies of about 5 MeV or more, but is observed for incident energies upward of the threshold given above. This is a complex mechanism and it takes place in the strong electric field of the protons in the nucleus of the atom.

The probability of each process with respect to energy of the incident γ-ray and Z of the material is summarized in Figure 1-5.

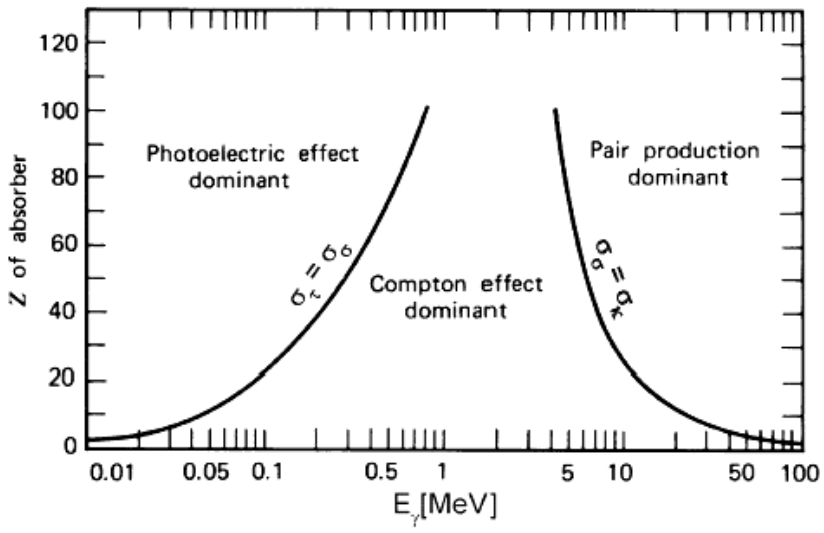

Figure 1-5 The importance of each interaction process with respect to incident energy and absorber Z. The lines indicate where the probabilities of the respective processes are the same [KNO01]

1.1.4 Thomson Scattering

No loss of energy is experienced when the γ-ray interacts with the absorber material. Since a change of direction is however experienced, this process is important for a complete radiation transport description with respect to energy deposition of the γ-ray.

1.1.5 Characteristic X-rays

The interactions discussed above (PE, CS and PP) lead to disruption of the atom when interaction with the photon occurs. The result is a temporarily excited atom. Rearrangement of the electrons involves electrons from a higher energy state filling the vacancy created by the ejection of a so-called Auger electron from the lower energy state. Associated with this rearrangement is the emission of a photon X-ray by the atom as it returns to a lower energy state.

1.2 Detecting gamma-rays: Predicted response functions

It was noted earlier that studying the gamma-rays emitted by nuclei will enrich our knowledge of the structure of the nucleus. It is therefore important that the gamma rays are detected in some form that allows for some kind of analysis that would achieve the aforementioned objective.

Ideally, when the gamma-ray interacts with a material, it should deposit all its energy without scattering out of the material. For a mono-energetic gamma-ray the differential distribution of the photon energy deposited will then be a simple spectrum as shown (Figure 1-6).

Figure 1-6 Ideal energy differential response function for a mono-energetic gamma-ray [KNO01]

If CS is taken into account the spectrum is changed as shown below (Figure 1-7), where a so-called Compton continuum is revealed between the extremes of the Compton Continuum at 180˚ and 0˚.

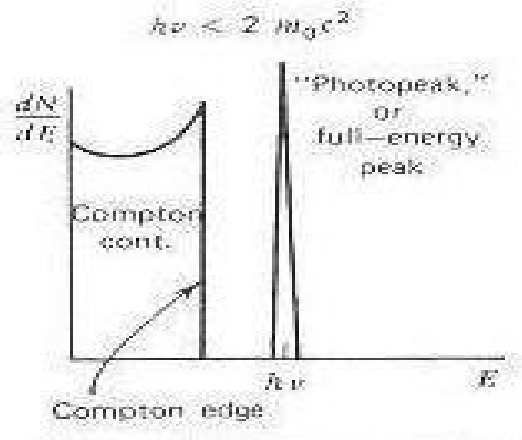

Figure 1-7 The Compton continuum that is due to scattering of gamma-rays out of the detector is shown above [KNO01].

PP introduces yet more complications into the simple differential distribution of particles with energy > $2m_oc^2$

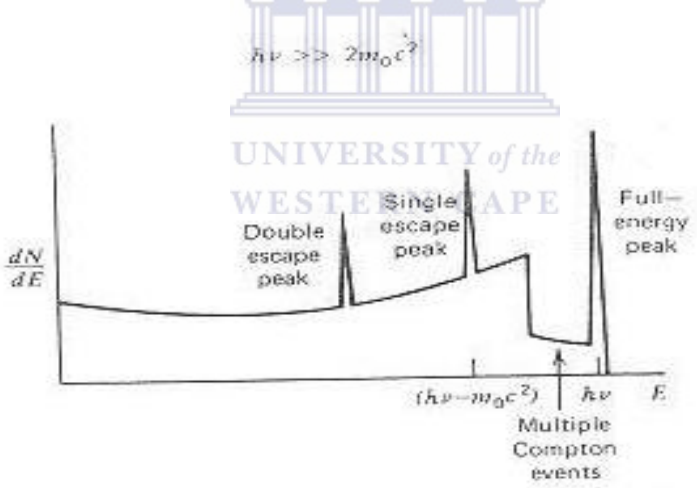

Figure 1-8 Spectral effects namely the single and double escape peaks that are due to Pair Production is shown here [KNO01].

One or both of the electron/positron pair may escape the detector which will lead to so-called escape peaks at the incident gamma energy less the electron rest mass or twice the electron rest mass. This is illustrated in Figure 1-8.

1.2.1 Detector response function and spectral features

It is well established that in order to detect gamma-rays, a detector must carry out two distinct functions. First, it must allow for a high probability of interaction between gamma rays and the detector and secondly, it must act as a conventional detector for the electrons that are ejected through interaction with γ-rays [KNO01].

This is due to the fact that all materials are invisible to gamma-rays i.e. gamma-rays cannot be detected directly, but are rather detected by measuring the electron response to the gamma-ray interaction within the detector material. An electric field applied to the detector material then aids in charge collection which in turn allows the measurement of energy deposited in the material.

1.2.2 Small detector response function

This is an example of one extreme in gamma-ray detector behavior. The detector is assumed to have small dimensions compared to the mean free path (MFP) of the Compton photons. Significant number of photons will therefore scatter out of the detector contributing to a large number of events resulting in a very high number of counts in the Compton continuum with a comparatively low number of counts in the photo-peak (see Figure 1-9).

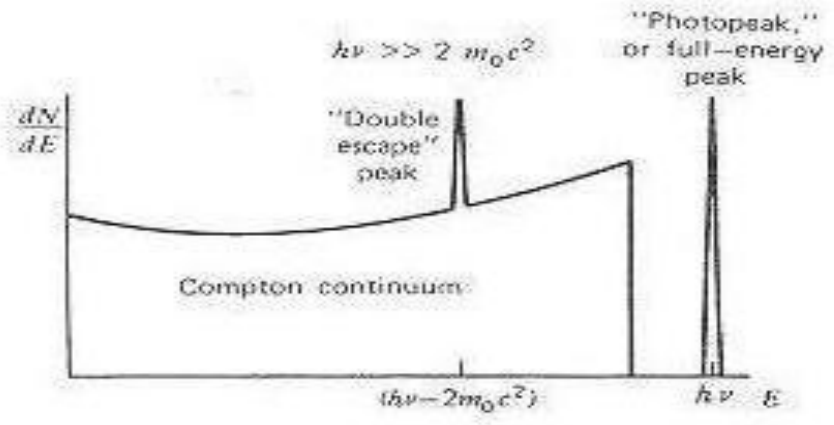

Figure 1-9 The resulting response function is shown above [KNO01]

1.2.3 Large detector response function

This is the other extreme where the detector dimensions are large with respect to the MFP of the Compton photons. In this instance we assume the detector dimensions are sufficiently large that no scattering out of the detector takes place.

The response function obtained is the ideal (similar to Figure 1-6) which reveals all the photo peaks with no Compton continuum.

1.3 Escape Suppression Spectrometers (ESS)

Real detectors are however of intermediate size and a Compton continuum will always be present. The extent of this continuum is dependent on the energy of the incident gamma ray and the detector size as well as detector material. Compton Suppression Spectrometers (CSS) have been designed to reduce the Compton continuum. This is necessitated by the Doppler broadening, ballistic effect, and neutron damage which are more pronounced in larger volume HPGe crystals.

A CSS consists of a heavy scintillator which captures a large number of the Compton photons that scatter out of the primary detector. Signals in the heavy scintillator, caused by the Compton photons that scattered out of the primary detector, are then used to veto signals in the primary detector if they are in coincidence, leading to a suppressed Compton continuum.

1.4 Gamma-ray spectroscopy with germanium detectors

Germanium detectors have very good resolution and for crystal sizes of about 7 cm length and 5 cm diameters, resolution are quoted at less than 2keV at 1.33MeV [DUC99]. It is for this reason that they are preferred over other gamma-ray detectors [KNO01, SHA1988, EBE08]. This is however a compromise since Z (number of

protons) for germanium is only 32; hence the interaction probability is not very high for gamma-rays of more than a few hundred keV.

Above 180keV, compared to the Photo-electric effect, Compton scattering becomes the dominant interaction mechanism. This effectively means that between 75-80% of interaction of gamma-rays still result in Compton events [SHA88, EBE08].

Germanium detectors initially had very small volumes since crystals of sufficient volume could not be grown between 1960 and 1970. This was due to the requirement for very pure germanium with impurities less than about 10^{10} atoms/cm^3. This is a direct result of the limited number of charge carriers produced per interaction which is about 1 per 2.9eV [EBE08] gamma-ray energy, which is still very low. To ensure efficient charge collection the impurities must therefore be very low.

Improvements in technology led to great improvements in germanium crystal quality to the extent that it replaced the lithium drifted germanium crystals commercially in the 1980's.

1.4.1 The high purity germanium detector

An HPGe detector is either p or n-type. Even at very high purity levels impurities of valence 3 or 5 still exist which acts as donors or acceptors to Ge with valence 4, compromising the charge collection process [EBE08]. Consequently a diode (detector) is built by doping n-type material which has an excess of donors with acceptors or vice-versa and by operating the diode with reverse bias. This creates an active volume that surpasses that which was obtained by drifting the germanium with lithium to result in the Ge(Li) detector.

The HPGe detector is a p-type detector - impurities are called acceptors - if it has lithium diffused into the outer surface of the crystal and boron diffused into the inner surface (see Figure 1-10 below), while for an n-type detector - impurities act as donors - the opposite is true.

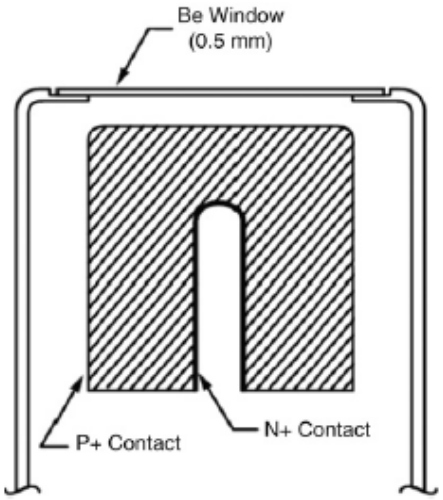

Figure 1-10 A typical n-type coaxial germanium detector [EBE08]

The germanium crystal is typically encapsulated in an aluminum end-cap and it is cooled by liquid nitrogen to reduce thermal noise produced by the diode leakage current in the detector system. Germanium detectors are treated in more detail in KNO01 and EBE08.

1.5 Monte Carlo Methods

The Monte Carlo (MC) method is a very powerful numerical technique that was first described (in its current form and approach) by Nicholas Metropolis and Stan Ulam [MET49].

In Monte Carlo transport calculations, the particle tracks or histories are created by simulating particle interactions with a material. To do this, one requires mathematical expressions for the probability relationships which govern the path length of a particle between interaction points, the choice of an interaction type at each such point, the choice of a new energy and a new direction if the interaction is of a scattering type, and the possible production of additional particles. These are all stochastic variables.

A complete understanding of the physics of the various processes a particle undergoes from the time it is "created" in the source until it is either absorbed or leaves the system under consideration, is required in order to make selections of the specific values for these variables.

Using "random" numbers, a computer can create a history of the life of each particle—similar to a random walk analysis. That is, an individual particle may experience many scattering interactions before finally being absorbed or escaping from the system. Random numbers—a set of numbers which have no pattern and are sampled uniformly between 0 and 1, are used at each interaction to determine which process occurs, how much energy is lost and the new direction of the particle (in the event of scattering).

The "life" of the particle begins when emitted by a source and ends with absorption or with a scattering event that moves the particle outside the region of interest. The events that occur during a particle's life are tabulated and become the history of that particle. Because a single particle is not representative of the system, a number of histories must be evaluated to accurately describe what occurs. Due to this statistical nature of MC, it is often a computationally expensive method to use. Its advantage is however that it can track particles in very complex geometries and the only uncertainties in the parameter of interest will be statistical.

This method can therefore be described as a numerical technique that uses random sampling to estimate the solution of a physical or mathematical problem.

A review of this method as a numerical technique up until 1970 is given by HALTON, 1970 [HAL70], which, while dated, contains the main ideas of the theory still relevant today. The use of this method as a technique to solve transport problems is described in Kalos and Whitlock, 1986 [KAL86] as well as by Hammersly and Handscomb, 1975 [HAM75].

1.5.1 Generic outline of the Monte Carlo Algorithm

A sequence of random numbers is used to produce a random distribution of quantities that simulate the problem at hand:

1. Determine the initial position where the particle is emitted.
2. Use a random number to select, the energy of a particle.
3. Use the next random number(s) to determine the direction of the particle's movement.
4. Use the next random number to determine the location of the next collision site (the distance traveled depends on the total cross-section of the material medium).
5. Check the new position to determine if the particle has escaped (leaked) from the system. If it has, add 1 to the total leaked and go to step 1 & start another history with another particle. If not, go to step 6.
6. Determine which type of interaction occurred at the new position, based on the next random number. Each type of interaction has an associated cross-section that determines the probability of occurrence:
    a. If the interaction is scattering, then determine the new energy of the particle after scattering using the next random number. Then go to step 3 & continue to follow the particle, i.e. determine the direction in which the scattered particle moves.
    b. If the interaction is absorption, go to step 1 and start a new particle in the system.
7. When a given set of histories has been completed—enough to provide acceptable statistical precision—evaluate the tally (quantity of interest).

A flowchart below outlines this method.

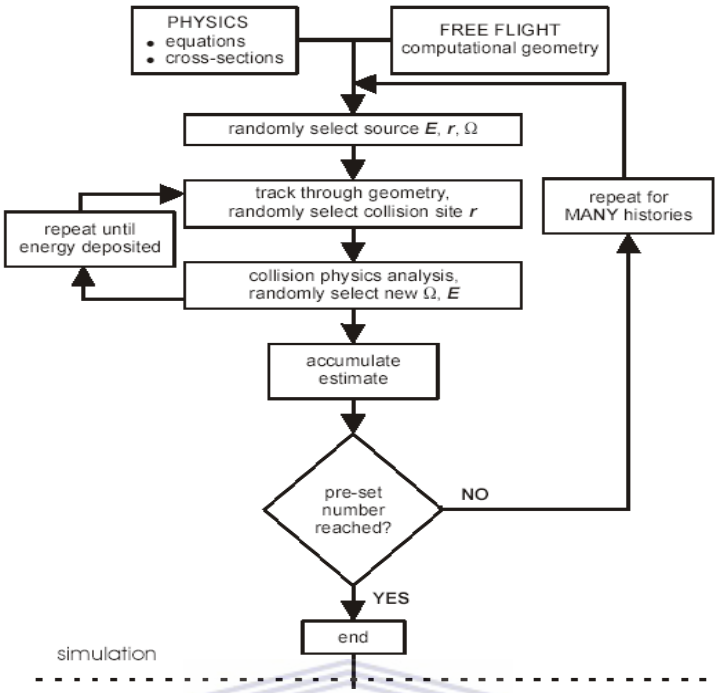

Figure 1-11 Generic outline of Monte Carlo algorithm [HEN03]

1.6 Scope and objective of this study

Gamma ray spectroscopy has provided large amounts of information on the behaviour and structure of atomic nuclei [SHA88, BEA92, EBE08]. Most of the major discoveries in experimental nuclear physics over the last five decades are strongly associated with improvements in detector technologies. Inorganic scintilators led to the discovery in 1963 of the first excited states of a rotational band based on the ground state of ^{162}Dy [SHA88]. Improvements in peak-to-background ratios as well as detector resolution obtained with germanium led to the first evidence of backbending which is associated with a two quasi-particle alignment in ^{160}Dy [SHA88].

Current ESS detectors can achieve a peak-to-total ratio of about 0.65 with Germanium as primary detector and Bismuth germanate (BGO) as the CSS for 1.332 MeV photons [SIM99].

This study investigates a new generation of HPGe detectors in a heavy scintillator shield that can hopefully achieve a Peak-to-Total ratio (P/T) of 0.80 for 1.332 MeV photons. These detectors are required for Nuclear Physics Studies with Radioactive Beams and will allow advances to be made in many other fields [SIM99, SHA08].

Scintillators, such as lead tungstate (PbWO), bismuth germanate (BGO) and lanthanum silicate (LSO), are finding wider uses in an expanding modern detector technology. A successful outcome to the present investigation, will give an opportunity of producing economically successful products that are of use in the nuclear and other industries as well as developing instruments for exploring new horizons in pure research [SHA08].

Modern generic computer programs, such as MCPNX [MAN05] and GEANT [AGO03], allow the efficacy of designs to be numerically verified without having to go to the expense of producing numerous prototypes [DUC99, SCH07]. Simulations can achieve high accuracy and the predictive power of these methods are well established [MIC86, DUC99, SCH07]. An initial concept for a new generation of detectors is shown in Figure1-12 below [SHA08].

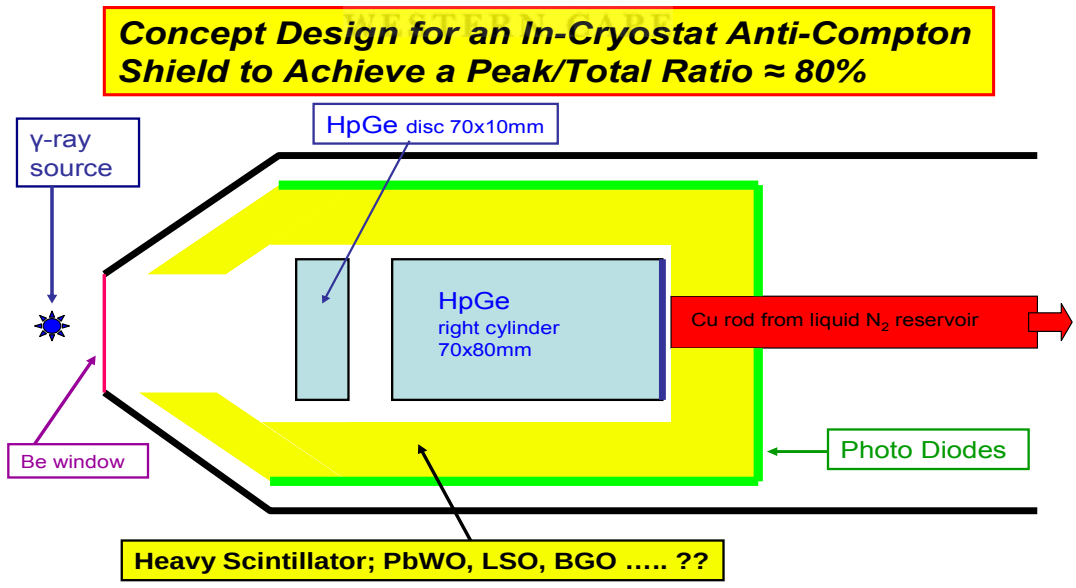

Figure 1-12 Schematic of concept detector to achieve Peak-to-Total (P/T) of 0.80 [SHA08]

As can be seen from Figure 1-4, a major contributor to the unsuppressed background is due to photons that enter the HPGe and immediately Compton scatter near to 180^{o} and exit through the opening through which they had entered. This is especially pronounced for gamma-rays of energy less than about 500 keV.

Such photons could possibly be suppressed by including a "thin" planar HPGe detector in front of the main HPGe detector, shown as a disc in the Figure. This detector would detect photons below 150 keV with high efficiency. Higher energy photons would pass through this detector with high probability and enter the main HPGe detector. Any such photons which were then backscattered out of the main detector would have an energy less than 250 keV (see equation 1.1) and be detected by the thin detector. Both the thin and the main detector would be operated in anti-coincidence with each other and with the CSS.

Numerical modeling of the system will initially investigate the optimum thickness and positioning of the "thin" detector, the geometry of the CSS and the location and detailed design of the Cu heat transport to the liquid nitrogen reservoir.

Summary of objectives of this study

1. Benchmark the MCNPX 2.5.0[1] transport package simulations of a (composite) Clover Detector [DUC99, see chapter two for more detail] at iThemba LABS against experimentally obtained measurements.
2. Investigate the effect on the Peak-to-Total ratio of placing a coincidence HPGe disc at the front of the current Clover detectors.
3. Investigate the performance of LSO and PbWO as ESS materials.
4. Investigate the effect of a back catcher on Peak-to-Total ratios.
5. Optimize the detectors to achieve a Peak/Total ratio of 0.80 for 1.332 MeV energy.

The above (2-5) will be investigated computationally using MCNPX 2.5.0.

[1] From hereon all references to MCNP or MCNPX refers to MCNPX version 2.5.0 used in this study.

1.7 Outline of this thesis

In Chapter 2 the experimental aspects and the simulation approach is outlined. Chapter 3 defines the parameters of interest as well as the analysis of the experimental results and the simulations. Conclusions are drawn about the use of MCNPX for this type of ESS design. In Chapter 4 the use of PbWO and LSO are modeled as the ESS of a clover detector with similar to that in use at GASP and Gammasphere. The effect of including back-plugs and an anti-coincidence shield in front of the detector is also evaluated. Chapter 5 is a review of the results obtained in Chapters 2-4.

CHAPTER 2 BENCHMARKING: THE MODELS

2.1 Experimental Aspects

2.1.1 AFRODITE detector array

The African Omnipurpose Detector for Innovative Techniques and Experiments (AFRODITE) (Figure 2-1 below) used in this benchmarking exercise became operational at iThemba LABS in January 1998. It is mainly used for investigating nuclear phenomena at high spin. This is done by measuring γ- and X-ray energies, yields and coincidence relationships associated with fusion-evaporation and fission reactions induced by heavy ions [NEW98].

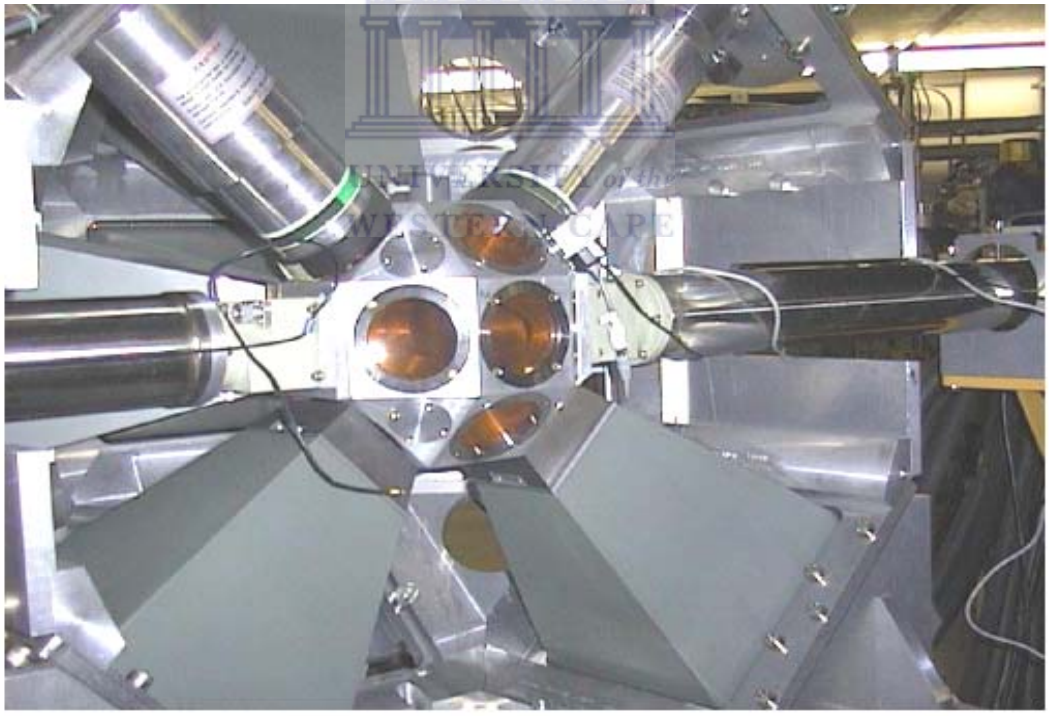

Figure 2-1 AFRODITE array at iThemba LABS

It can be operated with 8 Clover detectors [DUC99, NEW98] as well as 8 Low Energy Photon Spectrometers (LEPS) in the array or any combination thereof.

Although sixteen detectors can, in principle be accommodated, only fifteen are being used as the target ladder positioner is mounted on one facet. These are all arranged in a frame which has a rhombicuboctahedron shape. This frame consists of a main-body and an end-cap with a total of eighteen square facets at 0˚, 45º, 90º, 135º and 180˚ with respect to the beam direction.

Some specifications regarding these detectors are given below in Figure 2-2.

specification	Clover	Compton suppressors	LEPS
supplier:	Eurisys	Crismatec	Eurosys
number:	8	8	8
crystal type:	HPGe	BGO	HPGe
length:	71 mm[1]	~26 cm	10 mm
diameter:	51 mm[1]		66 mm[2], 60 mm[3]
thickness:		~(4-20)mm	
taper angle:	7.1°	~8.1°	
L_{ec}[7]:	20 mm		15 mm
entrance window:			119 mm[4]
L_{tc}[8]:			
total opening angle[4]:	23.2°		23.3°
detector solid angle[5]:	1.34%[6]		1.57%

before shaping[1]
external[2]
associated with the active area[3]
for a 4 mm gap between target chamber and end-cap.[4]
percentage of 4π[5]
for a 0.2 mm distance between crystals[6]
L_{ec} the distance from the detector end-cap to crystal surface[7]
L_{tc} the distance from the target centre to the crystal surface[8]

Table 2-2 AFRODITE array detector specifications [NEW98]

2.1.2 Clover Detector

As can be seen from the specifications in Figure 2-2 and the Figure 2-3, the Clover detector consist of four HPGe crystals, tapered at an angle of 7.1º at the front for two adjacent faces and the remaining faces are cut parallel to the crystal axis along its whole length. [DUC99]. This allows for close packing of the crystals with a distance of only 2mm between them. In order to optimize signal-to-noise-ratio the traditional aluminum used to house the detectors is not used, instead, a grip used at the back of

the detectors to keep them in position. The crystal has length 71mm and diameter 51mm before tapering and after tapering the diameter is about 41mm (50mm diagonally). The corresponding detector volume is about 470 cm^3 and about 89% of the original germanium volume.

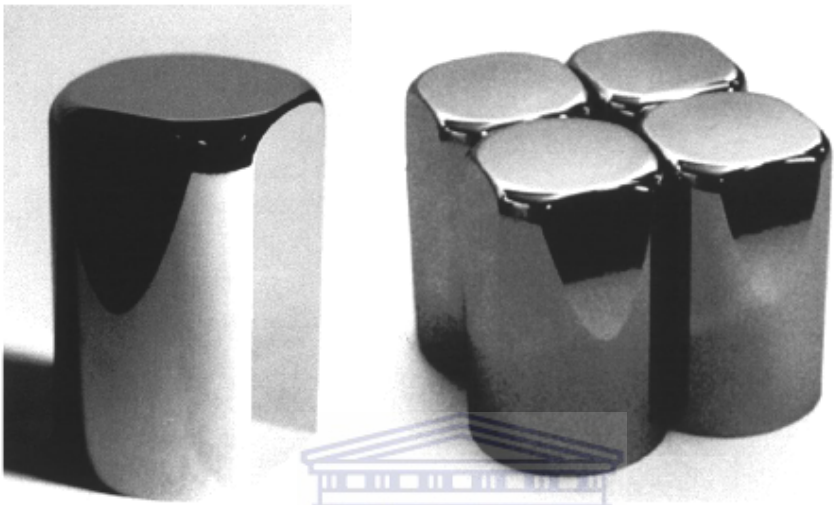

Figure 2-3 Individual crystal on the left and arranged as a Clover on the right [DUC99]

The detectors are housed inside a symmetric BGO Suppression Shield [Figure 2-4].

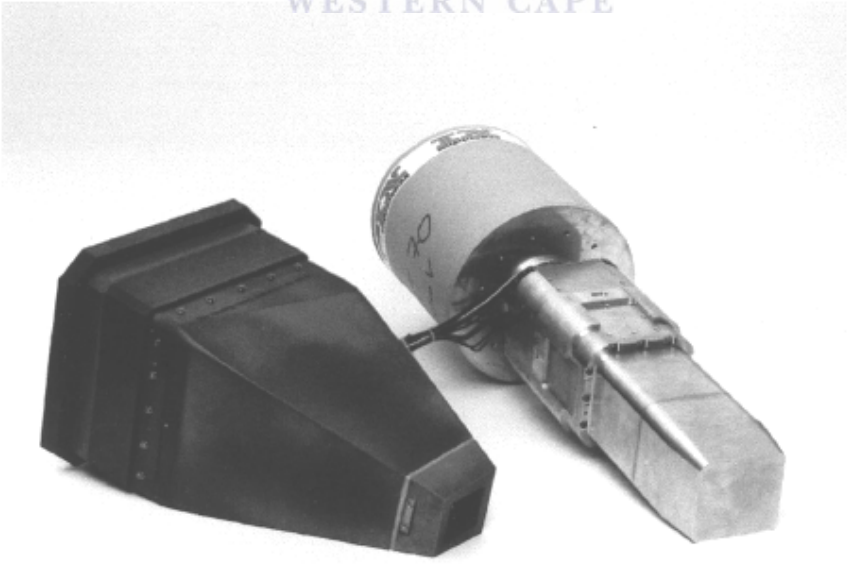

Figure 2.4 Picture of the BGO shield and assembled Clover [DUC99]

This shield has thickness 4 mm at the front and 20 mm at the back along all four sides

and actually consists of 16 individually mounted BGO crystals [NEW98, DUC99]. Each shield (individually mounted BGO crystal) is coupled to (a) Photo-Multiplier Tube (s) (PMT) and is shielded from γ-rays emanating from the target position with heavy metal (tungsten alloy) collimators. The signal from each of the PMT's for a specific shield are summed and used as a veto signal for the corresponding Clover.

2.1.3 Detection Modes

Gamma-rays can interact by depositing their energy in an individual crystal in what is known as the direct detection mode. In addition, due to scattering of gamma rays, interaction of a gamma ray in more than one detector is also possible. This is generically known as the add-back mode. In this mode of operation, the energy deposited is not measured directly but is coincidentally reconstructed. In the event that a gamma ray scatters into a transversally adjacent crystal in coincidence with another gamma-ray, the energy can be summed as if deposited in one crystal.

This gives rise to a number of ways in which data can be collected experimentally. The data at iThemba LABS is collected in three modes of operation which we describe with reference to Figure 2-5 below:

1. Any interaction in either of the elements 1 to 4 only is called the singles mode
2. The second mode of operation records events temporally in adjacent detectors namely, 1 and 2 or 2 and 3 or 3 and 4 or 4 and 1, the so-called doubles mode. This means that an interaction occurs in two and only two transversally adjacent elements, coincidentally. If a gamma-ray scatters out of 1 and 2 or 1 or 2 it would not be a double event.
3. The final mode implemented is the add-back mode. This is the sum of the interaction in 1 and only 1 element and doubles as defined in 2 above. The sum of the double events and the single only events is the add-back mode.

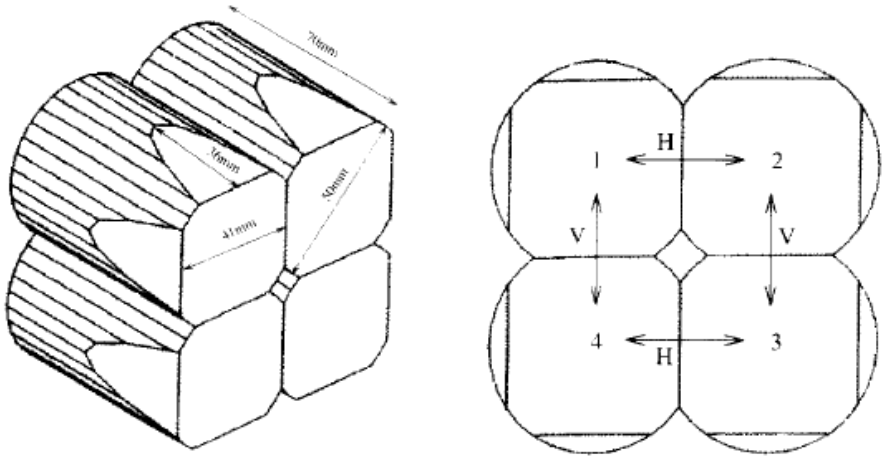

Figure 2-5 Schematic of the bare Clover crystals and detector [JON98]

All these modes of data collection were applied for each experiment carried out in this investigation.

2.2 The Experiment

2.2.1 Energy Calibration

Energy calibration of the detectors was done in the week preceding the experiment, with ^{152}Eu and ^{133}Ba sources and was confirmed every morning before data collection was done, with the same sources. These sources were placed on the target ladder inside the target chamber and the MIDAS Multi Instance Data Acquisition System [PUC07] (see http://npg.dl.ac.uk/MIDAS/) was used to facilitate data collection. The SFIT program was used to automatically find centroids of the photo-peaks. A polynomial of the form $E = a + bx + cx^2$ was used to associate a channel with a particular energy, where E is the energy and x is the channel number, and *a, b* and *c* are constant coefficients.

This process is in essence a mapping of a known energy to a known channel, from which the aforementioned polynomial is obtained. This then allows the determination of an unknown energy by simply identifying the channel where the centroid of its peak is located. This is done in a manner such that each channel will effectively

represent 0.5keV energy. This is standard procedure at iThemba LABS. This procedure is done for all individual elements of all clovers.

2.2.2 Gain Matching

Gain matching ensures that the same energy is collected in the same channel for the different elements of a particular clover detector. This is important to ensure add-back accuracy and hence the peak size determination.

2.2.3 Data taking: Source Measurements

Measurements of P/T have been performed using the γ-ray sources ^{60}Co, ^{137}Cs, and P/T - the ratio of the net peak counts and total counts - were then deduced offline for add-back, doubles and single hit modes. The activities of the sources were not known exactly although recorded on them was an original activity of 10μCi. The exact activity was however not of importance for the aspects under investigation.

2.3 Monte Carlo calculations

2.3.1 Physics models in MCNPX

The simulations for this investigation were done with MCNPX 2.5.0 [MAN05]. We noted earlier (section 1.5) that a detailed physics treatment is one requirement for accurate description of detector responses to radiation. In addition to this, the actual shape of the detector must be modeled as accurately as possible. The physics processes of importance, namely PE, CS and PP and TS have already been described in chapter one (sections 1.1-1.4) as well.

MCNPX provides for two physics treatments namely a simple physics treatment and a detailed (default) physics treatment. The simple physics treatment is more appropriate

to high energy (above 100 MeV) photons and was therefore not implemented for the simulations required in this study. The detailed physics model is the best model for most detector response simulations. Below we describe the approach taken in MCNPX with regard to photon interactions in both simple and detailed modes.

2.3.2 Photon Interactions

The interaction of photons with a material is implemented in one of two transport modes namely photon (P) or coupled photon-electron (P, E) mode, as chosen by the user. This is independent of the physics treatment (detailed/simple) implemented in the simulations. All photon interaction can cause the creation of electrons that are transported in the coupled electron-photon mode (mode P, E).

If electron transport is turned off (mode P), then a thick-target bremsstrahlung model (TTB) is used. This model generates electrons, but assumes that they are locally slowed to rest. In other words, energy losses occur at the point of interaction of the photon and electron. Any bremsstrahlung photons produced by the non-transported electrons are then banked for later transport. Thus electron-induced photons are not neglected, but the expensive electron transport step is omitted. (The TTB production model contains many approximations compared to models used in actual electron transport. In particular, the bremsstrahlung photons inherit the direction of the parent electron.)

The TTB approximation is the default for mode P problems. In mode P E problems, it plays a role when the energy cutoff for electrons is greater than that for photons. In this case, the TTB model is used in the terminal processing of the electrons to account for the few low-energy bremsstrahlung photons that would be produced at the end of the electrons' range.

2.3.3 Simple physics model

1. **Photo-electric effect** is treated as a pure absorption by implicit capture with a corresponding reduction in the photon weight[2], and hence does not result in the loss of a particle history except for Russian roulette played on the weight cutoff. The non-captured weight is then forced to undergo either pair production or Compton scattering. The captured weight is either assumed to be locally deposited or becomes a photoelectron for electron transport or for the TTB approximation.

2. **Pair production**: Two possible implementations of pair production are used in MCNPX. In a collision resulting in pair production an electron-positron pair could be created for further transport (or the TTB treatment) and the photon disappears. Alternatively it is assumed that the kinetic energy of the electron-positron pair produced is deposited as thermal energy at the time and point of collision, with isotropic production of one photon of energy 0.511MeV headed in one direction and another photon of energy 0.511MeV headed in the opposite direction.

3. **Compton Scattering:** This process entails scattering of the incident gamma-ray due to interaction with a free/atomic electron. To successfully describe this interaction type, the energy E' of the scattered photon must be determined as well as the angle through which the photon scatters. In this

[2] If MCNPX were used to simulate physical transport exactly, then each MCNPX particle would represent one physical particle and would have unit weight. However, for computational efficiency, MCNPX allows for techniques that do not exactly simulate physical transport, so-called variance reduction techniques. Particle weight is a number carried along with each MCNPX particle, representing that particle's relative contribution to the final tallies. Its magnitude is determined to ensure that whenever MCNPX deviates from an exact simulation of the physics, the expected physical result is preserved in the sense of statistical averages. Its usefulness is in the manipulation of the number of particles, sampling just a part of the problem to achieve the same results and precision without the need for a full unbiased calculation which has a longer computing time.

manner one determines the energy deposited at the point of collision as well as the new direction of the scattered photon. The energy deposited at the point of collision can then be used to make a Compton recoil electron for further transport or for the TTB approximation.

4. **Thomson Scattering:** Since scattering at high energies is highly forward peaked, this process is not implemented in the simple physics model.

2.3.4 Detailed physics model

1. **Photo-electric effect:** The incident photon is absorbed, several fluorescent photons are emitted and an orbital electron of binding energy $< E_\gamma$ is ejected (or excited), giving the electron kinetic energy E_e. The fluorescent photons are captured and eject electrons. All electrons produced are treated with the TTB approximation.

2. **Compton Scattering:** This process is modeled such that the scattering angle and energy of the photon is determined from the differential cross-section for a modified Klein-Nishina cross-section where the appropriate scattering factor decreases the cross-section (per electron) more extremely in the forward direction, for low E and high Z independently. The recoil kinetic energy is treated with the TTB approximation.

3. **Thomson Scattering:** Since no energy is involved with this process, only the scattering direction is calculated.

4. **Pair production**: This is considered in the field of the nucleus with a threshold of 1.022MeV. The electron and positron are created and treated with the TTB approximation. If the positron is below the electron energy cut-off, then a photon pair (0.511keV each) is created instead and its energy deposited locally.

2.4 Monte Carlo simulations of ESS

The Monte Carlo (MC) Method is a well established method to solve particle transport equations, in essence, the Boltzmann Transport equation. It has been used extensively in the design and evaluation of detectors [MIC86, BAX92, DUC99, SCH07].

Monte Carlo calculations were performed by a number of investigators to evaluate the full energy (FE), single escape (SE) and double escape (DE) intrinsic efficiencies of germanium detectors. These simulations showed the need for a complete and full physics treatment of the interaction of particles with matter for energies up to 12MeV. Further simulations showed the real active volume, excluding dead layers was crucial to reproduce FE peak efficiencies [MIC86 and references therein].

Compton Suppression Spectrometers (CSS) have been studied using Monte Carlo methods by e.g. Michel *et al.* [MIC86] using the EGRS program, and more recently the GEANT [AGO03] package was used by Duchene *et al.* [DUC99], Lipoglavsek *et al.* [LIP06] and Schumacher *et al*. [SCH07]. These calculations showed good agreement with the experimental results obtained for the CSS. It can therefore be stated with confidence that as a numerical method, MC is a useful tool for these simulations.

The general Monte Carlo Transport package MCNPX was recently used by Scates *et al.* [SCA06] in design studies of CSS's. It must be noted that the simulated Compton Suppression Factor and the experimentally obtained results showed that the simulated spectrometer detector had on average predicted a 20% better performance than eventually measured [SCA06]. This was ascribed to an underestimation of the dead material between detector and suppression shield.

2.4.1 The simulation approach

The Clover detector has already been modeled by Duchene *et al*. [DUC99] and

Lipoglavsek *et al*. [LIP06] with GEANT. Due to limited geometry options available in GEANT [AGO03], some approximations of the detector crystals, and hence the detector were required. The basic geometrical shapes available in MCNPX however made it possible to model the detector shape accurately with no approximations required. We investigated the P/T of the Clovers. As per the experimental aspects, gamma-ray energies, corresponding to the sources ^{137}Cs and ^{60}Co were modeled.

2.4.2 Clover Geometry

The Clover crystals have a complex shape that is difficult to reproduce in detail due to limited basic geometry capabilities in MCNPX. This was done by ensuring the full crystal area presented by the actual detectors was the same size in the model as that of the experimental setup. The volume and length of the crystals and hence the clover detector was maintained. Care was taken to ensure the detector volume and solid angle was preserved, but the dead layer of the detector was not included in the model. The model of the crystal simplifications is illustrated in Figure 2-6 below.

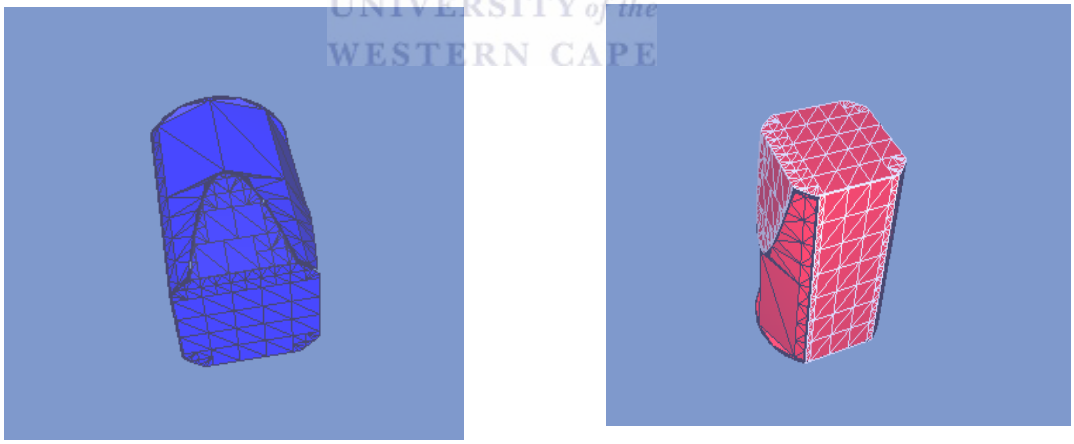

A **B**

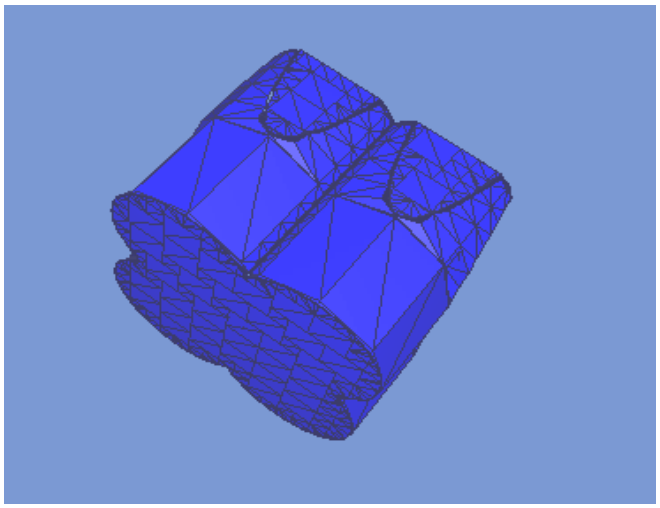

Figure 2-6 The MCNPX model of bare Clover elements shown in A and B as well as a bare Clover detector directly above

The BGO suppression shield was modeled accurately with all dimensions maintained. The model of the shield is shown in Figure 2-7 below.

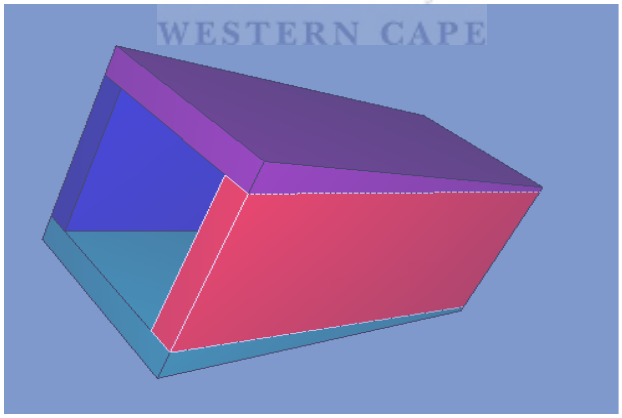

Figure 2-7 The BGO Suppressor Shield model used in the simulations

A model of the "bare" Clover and BGO shield is shown in Figure 2-8 below.

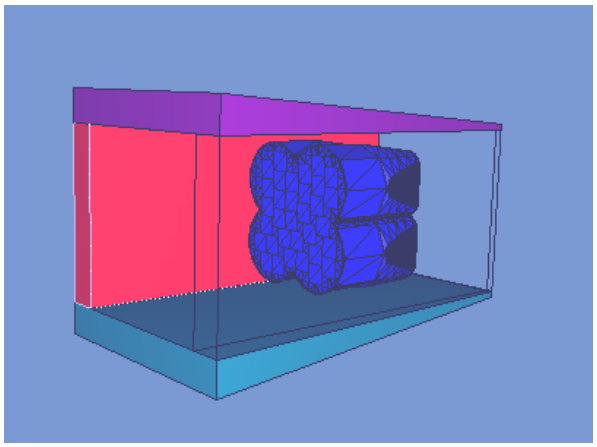

Figure 2-8 A cut-away view of the bare Clover inside the suppressor shield

2.4.3 Modeling the gamma-ray sources

The sources were modeled as point sources at a distance of 19.5 cm from the detectors in accordance with AFRODITE engineering drawings. The gamma-rays from the source were biased in the forward direction – gamma-rays were emitted in a forward direction limited to a solid angle of 24 degrees - to shorten the time required to obtain accurate statistics. Some approximations to the experimental set-up were made to reduce simulation time. The aluminum structure, beam line as well as the source positioner were not included in the simulation.

2.4.4 Modeling the collimator

In front of the suppression shields, 10 cm from the center of the target chamber, are 3cm thick tungsten collimators with a 3.5 cm by 3.5 cm opening for gamma-rays. The opening is tapered at 9˚. The collimator partially shadows the Ge crystals, but allows for smaller Doppler broadening of gamma-ray lines. The collimator shown in Figure 2-9 was modeled as the union of planes as surfaces.

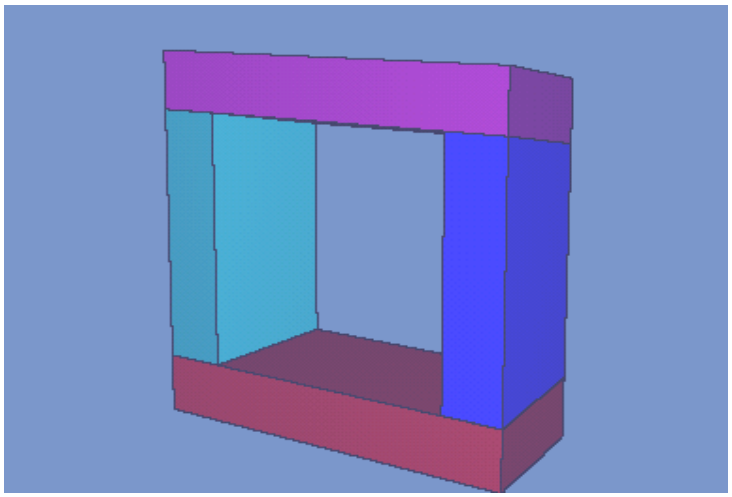

Figure 2-9 Rear view of the collimator comprising of four MCNPX cells

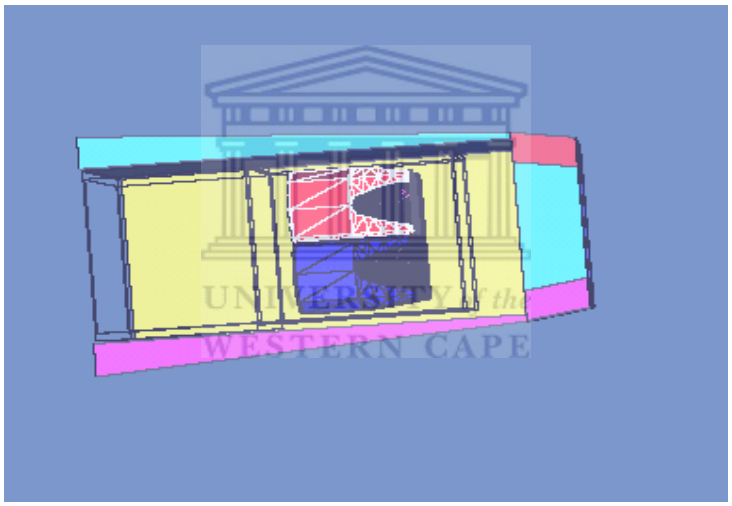

Figure 2-10 Top view of the complete MCNPX detector model with the top suppressor shield cut away

2.4.5 The pulse-height tally F8

The MCNPX pulse height tally F8, which records the distribution of energy deposited in a cell, was used to model the performance of the detector when the shield was "switched off". The special tally FT8 PHL was used to model the suppression by the BGO. They are described fully in MCNPX [MAN05] manual and are also described here for completeness.

The F8 tally allows for the modeling of detectors in that it tracks particles in the same manner that a physical detector would. The crystal of the detector is modeled as a so-called cell, in MCNPX parlance. A particle entering a cell would be tracked and the energy that is deposited in the detector, say in steps, would be summed, and put in the user specified energy bin, similar to an energy channel of an acquisition system that is used in experiments.

The cell in which the tallying i.e. energy deposition must be calculated, is specified on a so-called Tally Card. Say for example, that the cell that represents the crystal structure is labeled 1, then the Tally Card would have the command F#:*pl* 1, where ***pl*** is the particle type designator depositing energy in the detector, and # the tally type number. For the simulations under discussion the command would be F8:P 1. (Note: F8:P,E 1 and F8:E 1 are equivalent statements for an F8 tally in MCNP. Also see discussion above regarding the implementation of each in MCNPX above)

It is important to record that the F8 tally is limited to implementation in one cell and that it does not allow for the tallying to be divided on the basis of the nature of the interaction. This means that the modeling of the detector operated in different detection modes (see section 2.1.3) cannot always be simulated accurately. The singles as defined in section 2.1.3 can be replicated with MCNPX while the add-back modes can only be approximated.

2.4.6 The energy deposition tally F6

This tally allows the calculation of energy deposition in a cell of interest. It is an average tally, in the sense that it calculates average energy deposited in a cell and not the sum of all energy deposited in a cell.

2.4.7 The anti-coincidence tally FT8 PHL

This is a relatively new capability in MCNPX. It allows the calculation of suppression factors for ESS. With the FT8 special tally treatments card the F8 tally can become an

anticoincidence tally (FT8 PHL) or a different kind of tally altogether. This is illustrated by way of an example [MCK05], Figure 2-11 below.

```
Anticoincidence PHT 1 MeV Photons => Plastic/BGO
1 1 -7.130 -1        imp:p=1
2 2 -1.032  1 -2  3 imp:p=1
3 0         1 -2 -3 imp:p=1
4 0         2        imp:p=0

1 SPH 0 0 0 5.0
2 SPH 0 0 0 6.0
3 RCC -7 0 0 4 0 0 3.0

mode p e
sdef sur=2 nrm=-1 par=p erg=1.0
nps  100000
m1   83000 -0.671 32000 -0.175 80
m2   6000 -0.9153 1000 -0.0847
f26:e  2                $ Plastic energy dep.
ft26   GEB 0 0.1098 0
sd26   1
f36:e  1                $ BGO energy dep.
ft36   GEB 0 0.1098 0
sd36   1
f18:e  1                $ Plastic/BGO PHT
e18    0. 1.0
fu18   0. 99i 1.0
ft18   phl 1 26 1 1 36 1
fq18   u e
```

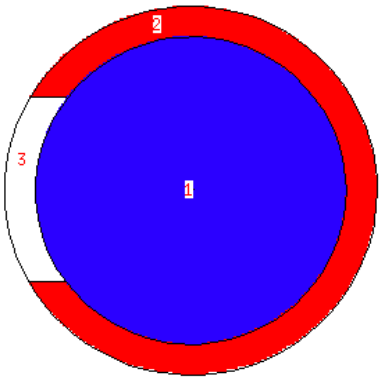

Figure 2-11 Typical MCNPX input file for ESS calculations [MCK05]

The following discussion concerns the text in red. Cell 1, which is the primary detector, is represented by the colour blue, cell 2, the suppresser shield, by the colour red and cell 3 by the colour white. The light output from two regions (cells 1 and 2) is used to subdivide the pulse-height tally. All the vetoed Compton (scattered) events are recorded by the FU8 tally in the bins of specified energy. In addition those events that are not in coincidence with events in cell 2 are treated as if they deposited all their energy in cell 1. Both the Compton events and the photo-electric events use the same bin format specified by the special tally command FU18.

With respect to the example above, a pulse of 0 is put into the first E8 bin and a pulse

of 1 into the first FU8 bin when the light output in cell 1 is < 0 MeV (no interaction in cell 1) *and* the light output in cell 2 is 0.01 MeV. This pulse is put into the second FU8 bin when the light output in cell 1 is < 0.01 MeV and the light output in cell 2 is between 0.01 and 0.02 MeV and so forth. These would be all the rejected (Compton) events.

A zero light output in both cells will result in no pulse height tally. A zero light output in cell 1 (tally 36) with a nonzero light output in cell 2 (tally 26) will result in a pulse in the corresponding FU8 bin.

Similarly, for a zero light output in cell 2 and a nonzero light output in cell 1, a pulse will be put into the corresponding E8 bin. Separate F6 tallies (F26 and F36) are needed since the two regions have different light conversion functions.

To summarize how this tally is implemented: Simplistically, if a particle interacts in cell 1 only, it is recorded as an event in the detector. An interaction in both cell 1 and 2 or cell 2 only is vetoed and rejected as a Compton event. An interaction in cell 1 only is recorded as an event irrespective of the energy deposited in cell 1.

2.5 Simulating single and add-back modes with MCNPX

The modeling of the unsuppressed and suppressed modes of operation for single mode detection is a straightforward implementation of the special anti-coincidence tally as illustrated in Figure 2-11 above. To simulate the add-back mode, with the union of elements 1 and 2 of Figure 2-5, one cell, say cell A, was formed and with the union of elements 3 and 4 also of Figure 2-5 another cell, say cell B. To ensure that events that occurred in cell A were doubles only, Cell B was used in anti – coincidence to cell A. This also meant that events that interacted in element 1 or 2 only was in this way also included in the tally, since again cell B would act as an escape suppression shield to any events that scattered out of 1 or 2. As defined in section 2.1.3 the sum of "pure" singles and pure doubles is the add-back.

Practically this means that we used half of the detector model as a representation of an entire Clover detector. This can be done due to proportionality. An increase of 4 in the number of events in the peak was offset by an increase in the number of events in the total. A complete definition of add-back as implemented in the detector is the sum of all possible double configurations, (4 in total), and the sum of all pure singles (4 in total), which is equivalent to the implementation of the add-back mode in the simulations.

2.6 Summary

In this chapter the experimental set-up and simulations were discussed alongside each other. It was shown, with reference to reported studies that Monte Carlo simulations are ideally suited to the design and optimization calculations for ESS. The methodology of the simulations was outlined where care was taken to reproduce the experimental set-up and then experiments as closely as possible. The input data used for some of the simulations are presented in Appendix A and B.

CHAPTER 3 BENCHMARKING:THE RESULTS

3.1 Data Analysis and Results

3.1.1 Parameters of Interest

Escape Suppression Spectrometers are characterized by Peak-to-Total (P/T) ratios. P/T is the net peak area divided by the total number of counts recorded in a spectrum for a particular nucleus. It is consequently energy dependent, since, as has been noted in chapter 1, all the interactions of interest, PE, CS and PP are dependent on the incident gamma-ray energy. It also depends on the resolution of the detector in question.

The convention is to define P/T for ^{60}Co and ^{137}Cs [KNO01, DUC99]. For ^{60}Co, it is defined as all the counts in both full energy peaks divided by the total number of counts above 100 keV up to and including the 1332 keV photo-peak. For ^{137}Cs it is defined as all the counts in the 662 keV full energy peak divided by the total counts in the spectrum, inclusive of the photo-peak.

3.1.2 Data Analysis

The experimental results were simultaneously recorded as the number of particles per energy (0.5 keV) interval, in singles- one element, doubles - two and only two elements - and add-back – sum of double and single only, interactions -, modes. The spectra obtained from the experiments were converted to Radware [RAD95] format which in turn was converted to ASCII files. This was done since the simulated results could not be changed into a form that could be analyzed with purpose built software, such as Radware [RAD95].

The simulated results are normalized, by default by MCNPX, to the number of starting particles. This means, instead of number of counts in the spectrum, the output is given as the probability that energy of a particular magnitude will be deposited in

the detector. P/T was directly calculated from the results. The simulated results were then normalized to the number of counts in the spectrum, so that a visual comparison between the results could be made.

3.1.3 Methodology used in Data Analysis

We now motivate the conversion of Radware compatible spectra to ASCII file. To calculate P/T, peak area determination becomes very important. It is therefore important that the results are evaluated in a consistent manner. When isolated and well resolved peaks are considered, simple numerical procedures can be used [KRA88]. This is usually done by subtracting the background from the spectrum obtained. A linear background may be assumed in uncomplicated spectra.

The peak area then simply becomes $\sum C_i$, where C_i is the number of counts per energy channel. The peak in this instance is determined mainly by visually searching for it. Alternatively, the magnitude of the peak area can be determined by fitting a Gaussian function to the peak area. The Gaussian function can be represented by

$$f(E) = Ae^{-(E-\bar{E})^2/2\sigma^2} \quad (3.1)$$

where A is a normalization constant. This equation can then be written as a linear equation

$$\ln(f(E)) = \ln A - \frac{(E_i - \bar{E})^2}{2\sigma^2} \quad (3.2).$$

A linear fit to this equation then gives the parameters $\bar{E}, \sigma$ and A. Integrating the Gaussian form then gives the net peak area as $\sigma A\sqrt{2\pi}$.

These simple procedures can only be used for relatively uncomplicated spectra. It was found for the data obtained with the experiments described in chapter 2 that both methods gave comparable results. The latter method was then used. This could be done due to the good resolution of the HPGe detector, which leads to well resolved peaks for ^{60}Co [KRA88, KNO01].

In the analysis presented here fairly simple techniques are used to determine the values of the parameters of interest. A word of caution is therefore appropriate: Backgrounds are often not well approximated by linear approximations and close lying peaks may overlap. Even the assumption of a Gaussian shape of the peak is often not correct. In these instances sophisticated fitting packages are more appropriate.

3.2 A limited review of Clover detector performance

The results obtained during this investigation must be put in context before an analysis of same is presented. The results (a)-(c) were reported by Lawrie *et al.* [LAW99] and that in (d) reported by Newman *et al.* [NEW98] in the Table 3-1 below.

	^{137}Cs 661 keV		^{60}Co 1332 keV	
	unsuppressed	**suppressed**	**unsuppressed**	**suppressed**
a	**0.22**	**0.31**	**0.13**	**0.21**
b	**0.32**	**0.52**	**0.20**	**0.37**
c	**0.35**	**0.53**	**0.23**	**0.41**
d	**0.38**	**0.57**		

a) sum of all clover elements, no add-back
b) sum of clovers for single element events (Compton scattered events rejected)
c) sum of clovers with add-back
d) same as (c) calculated by Newman *et al*. [NEW98]

Table 3-1 A summary of P/T values obtained for Clover detectors in single and add-back mode at iThemba LABS by Newman *et al*. and Lawrie *et al*.

The P/T values reported by Lawrie *et al*. and Newman ((c) and (d) in table above) differ when comparisons are made for ^{137}Cs with the detector operating in add-back suppressed and unsuppressed modes. An even bigger difference in P/T for unsuppressed (0.53) (Table 3-3) and suppressed (0.68) (Table 3-5) is seen when compared to the results obtained in this investigation.

In addition, when a graphical comparison was made between single, double and add-back mode, for the data obtained in this experiment, it became clear that there is

confusion in the nomenclature. The data labeled as double had a lower background than that of the add-back. Given that the add-back mode should have the lowest background, the results were then treated as follows: - the so-called add-back became our double mode and the double mode was changed to be the add-back mode. It then became clear that what Lawrie et al. and Newman reported as "add-back" mode is more comparable to what we term the double mode obtained in this experiment and from hereon will be treated as such.

A literature review of a series of studies [JOS97, LAW99, DUC99] with respect to the Clover detectors reveals some inconsistencies in the naming of events which lead to the differences in performance values obtained with the Clover detector.

Co-60	Peak-to-Total		
	Duchene [DUC99]	Joshi [JOS97]	Lawrie [LAW99]
Singles	0.16	0.10	0.13
Add-back	0.30	0.18	0.23

Table 3-2 A summary of unsuppressed P/T values obtained with Clover detectors.

The results of Duchene and Joshi were obtained with the source placed 25 cm from the detector surface and time shaping was the same, 6 μs.

As defined by Duchene, singles mode implies that each element is treated as a single detector. This means all events in an element are recorded. Joshi defines singles mode differently, namely as an interaction in one element, say element 1, only, with Compton events rejected. This also excludes events that scatter into element 1, by way of elements 2, 3 or 4 or any combination thereof. Note that for both Duchene and Joshi, the single mode would be analogously defined for elements 2, 3 and 4.

Thus, the singles mode of interaction is not defined in the same manner by Duchene *et al*. and Joshi *et al*. and the measured P/T is consequently different. The performance values reported by Duchene are arbitrarily used as reference values. Unsuppressed P/T reported by Duchene, 0.16 and Lawrie, 0.13 shows a large (about 18%) difference for seemingly similar detectors. Unsuppressed P/T reported by

Duchene, 0.16 and Joshi, 0.10 also show large but understandable (about 37%) differences as discussed above. These differences in unsuppressed P/T values are a consequence of the different definitions of the singles detection mode as discussed above.

The add-back mode can also not be compared directly due to differences in how this is defined. Joshi adds energies co-incidentally where 4 and only 4 elements fired whilst Duchene adds single hits to coincidental hits in multiple detectors. It is therefore clear from the P/T in add-back mode of Duchene and Joshi, that the manner in which data is collected (detection mode) does have an effect on the detector performance and this effect can be substantial.

Lawrie *et al*. defines add-back as the sum of a single interaction event only (see singles as defined by Joshi in this same section) and interactions in two and only two elements in temporal coincidence (see section 2.1.3). It is important to note that the definition and implementation of a particular detection mode has an effect on the performance values.

When the P/T of Newman and Lawrie are compared for ^{137}Cs, the effect of the threshold on the suppressor shield arises as an important issue. Newman set the detection threshold at about 40 keV while Lawrie had a detection threshold of about 65 keV. This means the detector shield with the higher threshold will not suppress scattered gamma-rays with energy below that threshold. This will make a difference in suppression performance, namely that the lower the threshold on the shield the more effective the suppression. This is seen (Table 3-1) in the difference in P/T obtained by Lawrie and Newman in doubles (what they referred to as “add-back” mode) mode. In theory, the lower the threshold the better, but in practice a very low threshold leads to a suppression of good events due to “noise” in the electronic circuits and random coincidences resulting from the background in the suppression shield.

It was previously shown [HIL86] that the effects of the threshold settings of the suppressor shield on the P/T can be significant. It was shown that the differences could be (approximately) as high as a factor 4 at lower energies between

100 to 200 keV, for thresholds of 15 and 100 keV respectively. Over the range of 100 to 700 keV the suppression varies approximately between a factor of 4 and 1 for the same thresholds of 15 and 100 keV. The effect of the threshold will be dependent on the suppression spectrometer, but what is clear is that the threshold will have a significant effect on P/T ratios.

This confirms the (systematic) effect experimental conditions have on performance values. To summarize: The methodology used to record the interactions of gamma-rays (detection mode definitions) in detectors as well as the experimental set-up, namely suppressor shield threshold, can lead to significant differences in the eventual detector performance.

3.3 Experimental and Simulation Results

3.3.1 Verification of the MCNPX clover detector model

	Mode	Experimental (E)	Simulated(S)
Cs-137	**Single**	0.24 ± 0.02	0.23
	Add-Back	0.53 ± 0.12	0.53[3]
Co-60	**Single**	0.13± 0.01	0.15
	Add-Back	0.40± 0.06	0.37[3]

Table 3-3 Experimental and simulated P/T values of Clover detector in single and add-back unsuppressed mode

Table 3-3 shows the experimental and simulated results with the Clover inside the BGO shield with the suppression capability switched off. The experimental results (Table 3-3) are stated with uncertainties and the simulations (Table 3-3) without. Uncertainties in the simulations are not indicative of the accuracy of the physics or

[3] It must be noted that the add-back simulated is not exactly as implemented in the experiment. In the simulation, events that scatter out of the cell for which tallying is done is suppressed, however, the FT8 PHT tally does not allow the suppression of events that scatter into the cell for which tallying is done from any adjacent cell. In the experiment the latter is also done.

geometric models used in the simulations but rather the precision that can be obtained with the Monte Carlo technique. The precision of Monte Carlo methods, due to the mathematical basis of the technique, is only limited by the computationally expensive implementation of the technique. The uncertainties in the experiment, in theory includes both systematic and random errors, hence P/T values for the experiment is stated with uncertainties. It is important however to note that as the interactions of radiation with matter is also a statistical/random process, the uncertainties stated in Table 3-3 for the experimental results are (probably) mainly due to the number of events recorded.

Good general agreement is obtained for the simulated single mode for both Cs-137 and Co-60. Given that for the single mode, the methodology used to generate the response function is the same as that implemented in the experiment, it gives us confidence that the detector model, with approximations as outlined earlier, is a satisfactory geometrical model of the actual detector.

The same does not hold for the add-back mode. As outlined earlier (footnote page 50), the simulation and experimental add-back mode is slightly different. For the simulations, the Compton background contains more events due to the in-scattering of gamma-rays from cells adjacent to the cell in which tallying (counting) occurs. In the experiment these in-scatterings are suppressed leading to a lower background. Taking this into account, the general agreement between experimental and simulated results is good. At lower energies Compton scattering is less likely to occur, hence the effect of the in-scattering is not noticeable in the P/T calculated for ^{137}Cs but is noticed in the P/T for ^{60}Co.

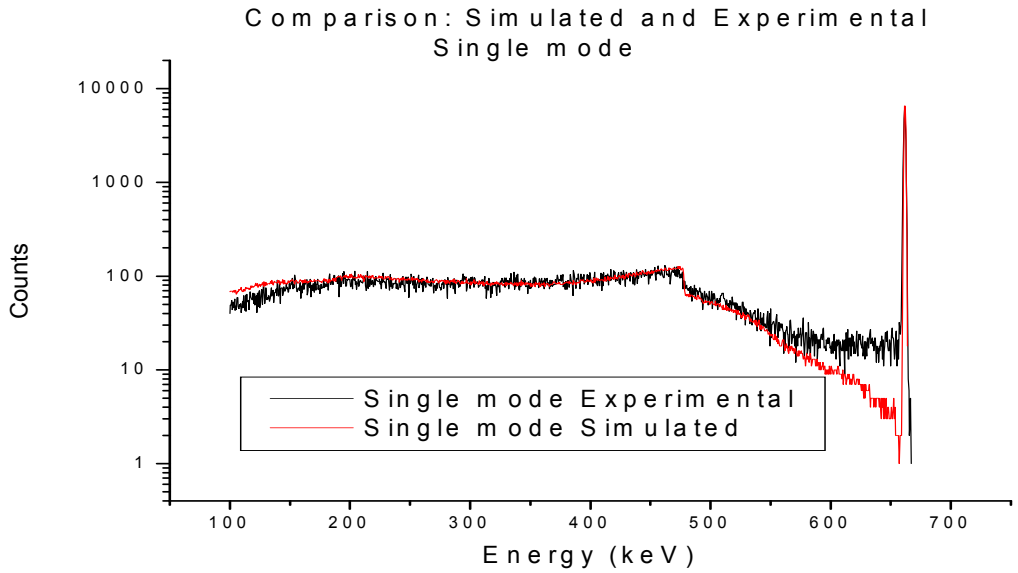

Figure 3-4 Experimental and Simulated (normalized to counts) response function unsuppressed

The agreement between simulated (normalized to counts) and experimental response function (Figure 3-4) is good. At energies below approximately 180 keV however, differences are clearly seen in Figure 3-4. Forward-scattering of gamma-rays plays an important role in this region. The difference could be attributed to the lack of a co-axial and outer dead-layer (especially at the back, where electronics may lead to a reduced detector volume) in the detector model implemented in MCNPX. At lower energies (below 180 keV), gamma-rays are more likely to undergo photo-electric effect, that is, in forward scattering events, the energy deposited in the detector will be below 180 keV and is therefore more likely to be captured in a dead-layer. At energies below 180 keV the effect of the dead-layer would therefore be noticeable.

The differences in the response function between 550 and about 650 keV can probably be ascribed to a lack of dead layer in the simulations as well. In this region of the response function, multiple interactions (Compton scattering) (see Figure 1-8) play an important role [KNO01]. As multiple interactions also include co-incidental interactions between elements, the co-axial and outer dead-layers would play an important role in "capturing" scattered gamma-rays, which, especially for ^{137}Cs, would have low energy.

The simulated detector in this region is therefore more efficient and multiple interactions is now summed and shifted to the peak. This would reduce the number of events recorded in the region where multiple scatterings dominate (550 to 650 keV). The effect on the simulated peak is however minimal when a comparison is made between simulated and experimental photo-peaks. It was shown by Sima *et al.* [SIM09] that simulated detector efficiency could be higher than the actual experimental efficiency if the detection threshold in the simulations is set low. At low energies if no threshold is applied, as is done in the simulations presented here, the simulated detector efficiency are higher than that of the actual detector at lower energies.

We now state the minimum criteria which must be met so that experiment and simulations agree. Various investigators [MIC86, LAB00, DAM01] have shown that in order to obtain good FEP efficiency agreement between simulated and experimental results, detailed information regarding detector geometry is required. Further, physics models implemented must be as accurate as possible and lastly, the experimental process must be reproduced as closely as possible.

It was shown [VEN05, DUC99, SCH07] that when complete information regarding detector geometries are available, agreement of experimental and simulated detector responses are very good. It would then seem that since incomplete information regarding the detector geometry was available, in this investigation, specifically with respect to the dead-layer dimensions the efficiency of the simulated detector would be inaccurately reproduced. P/T is linked to the efficiency of the detector and discrepancies in detector efficiencies would lead to discrepancies between simulated and experimental P/T results.

3.3.2 Verification of the MCNPX suppression mode results

The simulated and experimental results for the Clover detector in single and add-back mode are summarized in Table 3-5 below for the case when suppression is included.

	Mode	P/T Experimental (E)	P/T Simulated(S)
Cs-137	**Single**	0.29	0.31
	Add-Back	0.68	0.81
Co-60	**Single**	0.23	0.23
	Add-Back	0.54	0.64

Table 3-5 Experimental and simulated P/T values of Clover detector in single and add-back suppressed modes

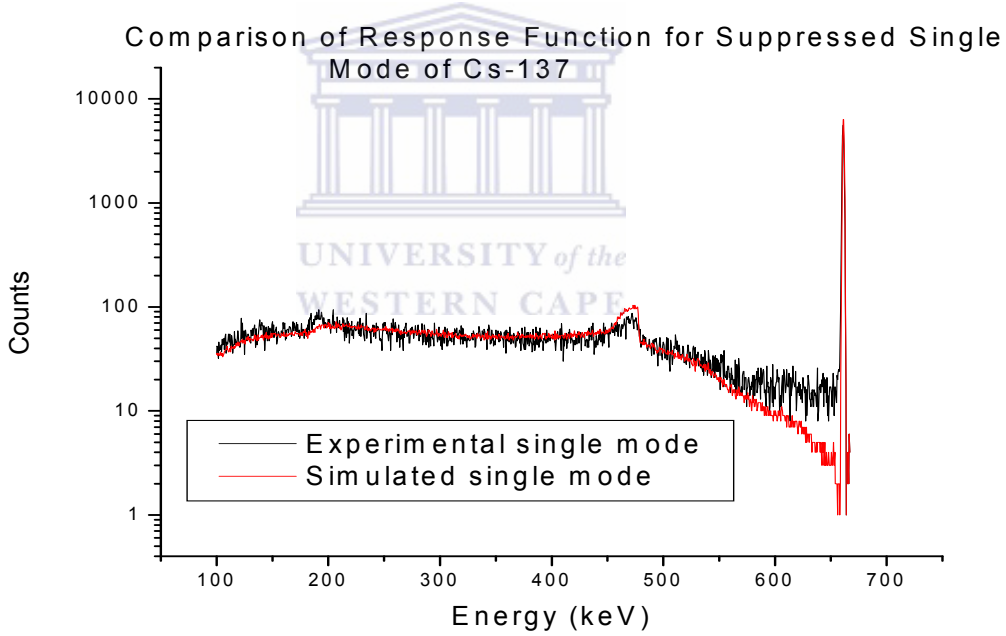

Figure 3-6 Typical response functions-simulated and experimental- for Cs-137

We note the excellent agreement between single mode results in Figure 3-6. In add-back mode the difference in P/T (Table 3-5) is also clear. Just as for the unsuppressed results, we are confident that the geometrical model of the BGO shield is a reasonable approximation. As noted, the simulation of the single mode is exactly

as it is implemented in the experiment. The suppressor shield is also expected to operate exactly as modeled.

Some differences in shape of the response function can be seen though in Figure 3-6 above. At the Compton edge, suppression is better in the experiment compared to the simulation. This could be due to lack of co-axial hole and dead-layer in the modeled detector geometry. The dead-layer in the co-axial region would be effective at capturing some of the backscattering gamma-rays. Hence, when it is not included in the simulations, more events would be counted/captured in the simulation compared to the experiment.

Given the agreement of the suppressed results for the P/T in single mode, the question arises as to the discrepancy between absolute P/T values in add-back mode. We now propose a qualitative explanation for the discrepancies as seen in the stated results above. This is done since, as stated, the modeled add-back mode is only an approximation to the actual experimental implementation of these modes of operation.

It is easily seen that in add-back mode, the scattered gamma-ray will generally be of lower energy than the singles mode. Lower energy gamma-rays and high Z material (BGO) makes full energy absorption more likely. The suppression of scattered events in the experiment will therefore be affected by the detection threshold on the BGO shield.

Experimentally, the threshold will play an important role **(**see section 3.2 above). All events, scattered out of the detector which interact with the shield, below the threshold will not lead to a reduction in the back-ground. In the simulations however all scattered events that deposit energy in the shield will lead to suppression. A consequence of this is possibly a higher suppression when interaction occurs in add-back modes as simulated compared to experimental.

In add-back mode, due to scattering, the energy of the scattered gamma-rays in the crystals will have low to very low energies. Experimentally, a threshold will have been set on the detection limit on the HPGe elements as well. This means that while in

the simulation, these events add to the full-energy peak events, the peak will be reduced experimentally.

3.4 Summary

The experimental results for direct (singles) and indirect (add-back) detection modes were compared. The agreement in the absolute values of P/T for the single mode is acceptable. This implies that the geometrical model of the bare crystal detector model is acceptable. The same is true about the implementation of the suppression mode for single direct detection. It was shown that MCNPX[4] can be used to model the direct detection mode of composite detectors in both suppressed and unsuppressed mode.

The simulation of the add-back mode is not as straightforward as for the singles mode due to limited capability of the pulse-height tally in MCNPX. It can only be implemented in one cell or alternatively in two cells as the special tally FT8 PHL, where the pulse-height tally becomes an anti-coincidence tally based on energy deposition in two regions. It was therefore not possible to implement the add-back mode exactly in the simulations.

Further, it is not possible to implement energy cut-offs in two regions. It therefore becomes difficult to appropriately implement the experimental conditions, which require the implementation of detection thresholds for the detector and shield. (It is possible to implement energy cut-offs with the F8 tally but not with the special FT8 PHT anticoincidence tally). This will lead to better suppression in the add-back mode, as simulated compare to the experiment, due to the fact that no threshold is put on the suppressor shield in the simulation. This means the simulated suppression will be more effective compared to the experiment.

The agreement between simulated and experimental results is therefore good. The simulated P/T in add-back suppressed mode should be considered the ideal

[4] It should be noted that this discussion and all others in the text refers to the version of MCNPX used in this investigation namely MCNPX 2.5.0.

performance possible with Clover detectors [MIC86]. It can be concluded that subject to the detection mode implemented in actual composite detectors, MCNPX, can be used to design and project the performance values of composite detectors.

CHAPTER 4 SUPPRESSOR SHIELD EVALUATION

It has been noted earlier that Lanthanum silicate (LSO) and Lead tungstate (PbWO) are possible candidates for use as shields in escape suppression spectrometers (ESSs) [SHA08]. In this Chapter we report on the simulated effectiveness of these materials compared to BGO in this chapter. In addition, we consider the effectiveness of adding a back-plug and planar detector at the front of the detector.

4.1.1 Detector Geometry

The modeling of the Clover detector became computationally very expensive when the add-back mode was simulated. In order to make the modeling computationally less expensive for the evaluation of LSO and PbWO as suppression shields, the basic detector geometry has been simplified compared to that of the Clover model. The detector crystal is generically similar (in terms of detector and suppression shield shape, but not dimensions) to those employed in EUROGAM I and GASP. The detector was modeled as a single crystal, diameter 9 cm and length 11 cm. It was tapered at 5 degrees from about halfway along its length as demonstrated in Figure 4.1.

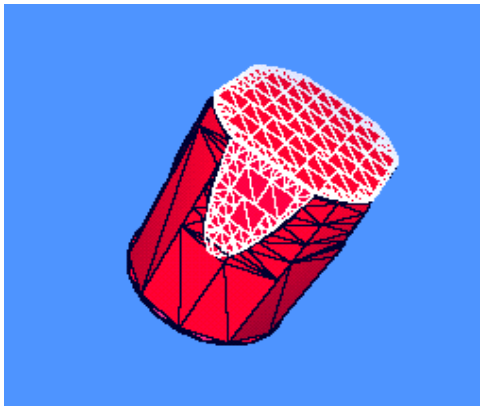

Figure 4-1 Bare detector crystal tapered at 5 degrees from about halfway along its length of 11 cm

The detector crystal was then put inside an aluminum can of thickness 1.5mm. The shield shown in Figure 4-2 below was constructed in a similar manner to that used in the Clover detector. The thickness was kept constant at 5 mm at the front and varied between 5 mm and 20 mm at the back.

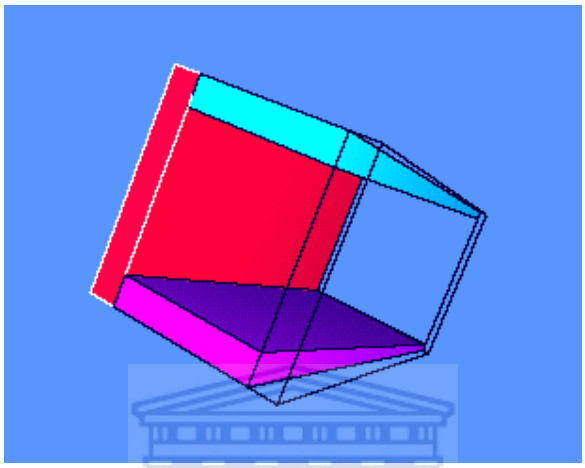

Figure 4-2 Geometry of the shield used in the suppression calculations

The detector was then placed inside the suppression shield, at a distance of 6 cm behind the front of the shield.

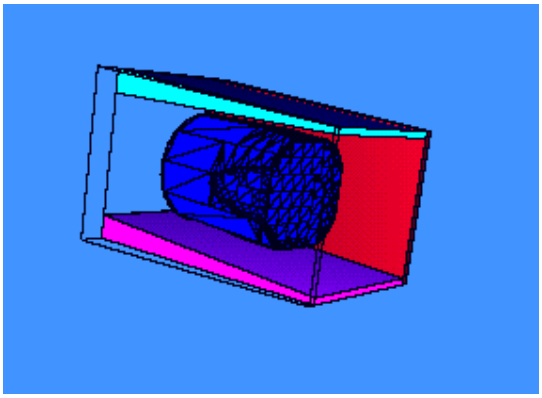

Figure 4-3 The bare crystal positioned inside the detector shield with one side of the shield made transparent so that the detector crystal is clearly visible

4.1.2 Modeling the gamma-ray sources

The sources were modeled as point sources at a distance of 19.5cm from the detector surface. The gamma-rays emitted were biased in the forward direction to shorten the time required to obtain accurate statistics.

4.2 Results and Discussion

	Shield	5 mm	10 mm	15 mm	20 mm	Back-Plug 40 mm	Front Disc 10mm
Co-60	LSO	0.62	0.65	0.67	0.68	0.68	0.69
	PbWO	0.70	0.75	0.78	0.80	0.81	0.81
	BGO	0.69			0.81		

Table 4-4 P/T ratios for varying thickness of shield thickness of LSO and PbWO referenced with BGO at two thicknesses

PbWO has been shown to be more effective as a suppressor material than LSO. The performance of PbWO mirrors that of BGO and could replace it as a shield if appropriate. It is not surprising that BGO and PbWO gives similar performance as the average Z values are approximately the same.

Surprisingly, the back-plug does not lead to any improvement in P/T. Surprising, since for Gammasphere an improvement of 10% in P/T was measured [BAX92] when compared to without a back-plug. This is probably due to the increased length (11 cm) and radius (4.5 cm) of the detector simulated in this investigation, compared to Gammasphere (length > 7 cm radius approximately 3.5 cm) or GASP (similar dimensions as Gammasphere). Gamma-rays that scatter forward will be more likely to interact again in the detector crystal compared to those used in Gammasphere/GASP. The effect of the back-plug is consequently reduced in the simulations presented here. The efficiency of the detector in this simulation will therefore be improved compared to Gammasphere. The P/T ratio will therefore increase just as a consequence of the detector dimensions.

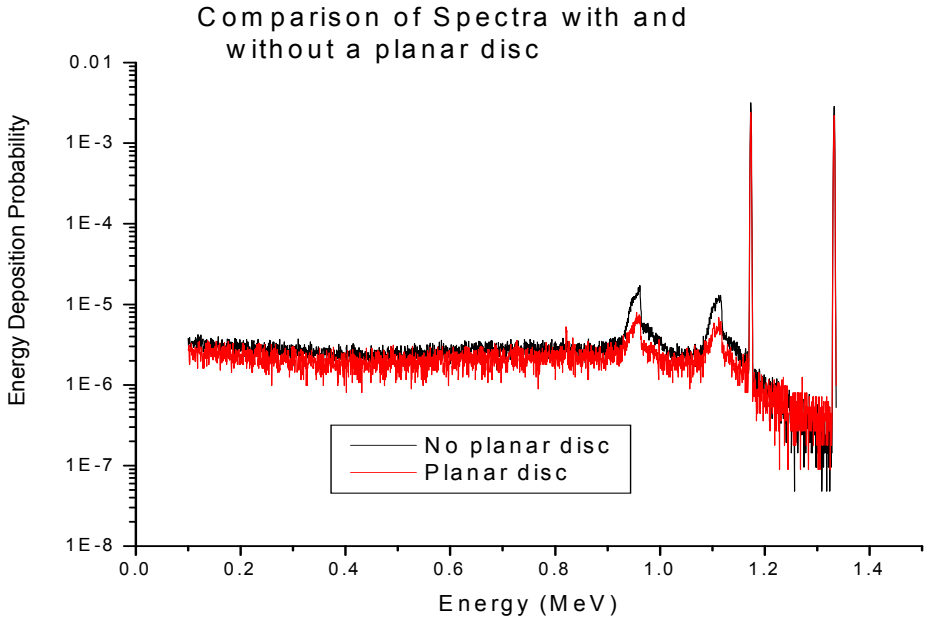

Figure 4-5 Comparison of Spectrum with and without a planar disc in front of main detector

The planar disc in front of the detector does lead to an improvement of 1% in P/T overall. The effect is more clearly seen in Figure 4-5 when we do a graphical comparison between the P/T at 20mm (see Table 4-4 for P/T at 20 mm) and that obtained with same and the front disc (see Table 4-4 for Front Disc 10 mm). For energies below 150 keV an improvement of up to 60% is calculated.

4.3 Conclusion

LSO and PbWO were compared to BGO as possible suppressor shield materials. It was shown that PbWO compared favorably with BGO while LSO give much weaker suppression. This is not unexpected since the average Z for LSO is much lower than for PbWO and BGO, the latter being comparable.

Unexpectedly, the inclusion of a back-plug did not improve the P/T. This is ascribed to the increased detector dimensions simulated in this study compared to that of the detectors used in Gamasphere/Gasp. The addition of the front disc improved P/T by 1%. The effect is however better appreciated when a comparison is made at lower energies (below 150 keV), where a lower background of up to 60% is calculated.

CHAPTER 5 SUMMARY AND CONCLUSION

5.1 Summary and Conclusion

In this investigation we set out to evaluate the use of MCNPX to model complex composite detector performance. Furthermore, LSO and PbWO were compared with BGO as possible suppression shield materials.

It was concluded, with reference to studies reported in the literature, that when complete and full information regarding detector geometry is available, the direct detection mode (as defined by Duchene [DUC99] and Lawrie [LAW99]), can be accurately modeled with Monte Carlo based techniques. Designers of detectors can therefore use MCNPX as a design tool to optimize detector performance and a prototype could be build on the basis of these simulations.

Very good agreement between prototype and MCNPX model is expected if the geometrical model is a good description of the detector. In addition, better agreement is possible if the experimental environment could be included in the model in as much detail as possible. The latter may however lead to very long simulation run times.

Composite or add-back modes are not well described by simulation done with MCNPX. This is in the main due to the limitation of MCNPX 2.5.0 to implement the exact composite experimental detection modes. Suppression is overestimated with MCNPX since a detection threshold cannot be implemented on the suppressor shield. Performance values should therefore be treated with caution for composite detectors, especially in suppressed mode, since detection threshold cannot be implemented in the simulation.

Addition of a back-plug does not lead to a lower background in our simulations whereas the addition of a planar disc at the front of the detector does lead to an improvement in P/T of 1%, with an especially a noticeable effect below 150keV.

REFERENCES

[AGO03] S. Agostinelli, J. Allison, K. Amako, J. Apostolakis, H. Araujo, P. Arce, M. Asai, D. Axen, S. Banerjee, G. Barrand, F. Behnerl, L. Bellagamba, J. Boudreau, L. Broglia, A. Brunengo, H. Burkhardt,S. Chauvie, J. Chuma, R. Chytracek, G. Cooperman, G. Cosmo,P. Degtyarenko, A. Dell'Acqua, G. Depaola, D. Dietrich, R. Enami,A. Feliciello, C. Ferguson, H. Fesefeldt, G. Folger, F. Foppiano, A. Forti, S. Garelli, S. Giani, R. Giannitrapani, D. Gibin, J.J. G!omez Cadenas, I. Gonz!alez, G. Gracia Abril, G. Greeniaus, W. Greiner, V. Grichine, A. Grossheim, S. Guatelli, P. Gumplinger, R. Hamatsu, K. Hashimoto, H. Hasui, A. Heikkinen, A. Howard, V. Ivanchenko, A. Johnson, F.W. Jones, J. Kallenbach, N. Kanaya, M. Kawabata, Y. Kawabata, M. Kawaguti, S. Kelner, P. Kent, A. Kimura, T. Kodama, R. Kokoulin, M. Kossov, H. Kurashige, E. Lamanna, T. Lamp!en, V. Lara, V. Lefebure, F. Lei, M. Liend, W. Lockman, F. Longo, S. Magni, M. Maire, E. Medernach, K. Minamimoto, P. Mora de Freitas, Y. Morita, K. Murakami, M. Nagamatu, R. Nartallo, P. Nieminen, T. Nishimura, K. Ohtsubo, M. Okamura, S. O'Neale, Y. Oohata, K. Paech, J. Perl, A. Pfeiffer, M.G. Pia, F. Ranjard, A. Rybin, S. Sadilov, E. Di Salvo, G. Santin, T. Sasaki, N. Savvas, Y. Sawada, S. Scherer, S. Sei, V. Sirotenko, D. Smith, N. Starkov, H. Stoecker, J. Sulkimo, M. Takahata, S. Tanaka, E. Tcherniaev, E. Safai Tehrani, M. Tropeano, P. Truscott, H. Uno, L. Urban, P. Urban, M. Verderi, A. Walkden, W. Wander, H. Weber, J.P. Wellisch, T. Wenaus, D.C. Williams, D. Wright, T. Yamada, H. Yoshida, D. Zschiesche, *Nuclear Instruments and Methods in Physics Research* A 506 (2003) 250-303

[BAX92] Baxter A.M, Khoo, T.L, Bleich M.E, Carpenter M.E, Ahmad I, Janssens R.V.F, Moore E.F, Bearden I.G, Been J.R, Lee, I.Y, *Compton Suppression tests on Ge and BGO prototype detectors for*

Gammaspere, Nuclear Structure at High Angular Momentum, Ottawa, Canada, May 1992.

[BEA92] Beausang C.W, Forbes S.A, Fallon P, Nolan P.J, Twin PJ, Mo J.N, Lisle J.C, Bentley M.A, Simpson J, Beck F.A, Curien D, deFrance G, Duchene G, Popescu D, *Measurements on prototype Ge and BGO detectors for the Eurogamm array,* Nuclear Instruments and methods in Physics Research A 313 (1992) 37-47.

[DAM01] Damon, RW, *Determination of the photo-peak detection efficiency of a HPGe detector, for volume sources, via Monte Carlo simulations*, MSc Thesis (2001),University of the Western Cape, unpublished.

[DUC99] Duchene G, Beck F.A, Twin P. J, de France G, Curien D, Han L, Beausang C.W, Bently M.A, Nolan P.J, Simpson J, *The Clover: a new generation of composite Ge detectors,* Nuclear Instruments and methods in Physics Research A 432 (1999) 90-110.

[EBE08] Ebert J, Simpson J, *From Ge(Li) detectors to gamma-ray tracking arrays- 50 years of gamma spectroscopy with germanium detectors,* Progress in Particle Physics 60 (2008) 283-337.

[HAL70] Halton J.H, *A retrospective and prospective survey of the Monte Carlo Method,* SIAM REVIEW VOL. 12, No 1, January 1970.

[HAM75] Hammersley J.M, Handscomb D.C, *Monte Carlo Methods,* 1975, London: Methuen & Co, Edited by MS Bartlett.

[HEN03] Hendriks P.H.G.M., *In – depth γ – ray studies – Borehole measurements*, University of Groningen, PH.D Thesis (2003), pp 62 – 63, 69 – 71.

[JON95] Jones P.M, Wei L, Beck F.A, Butler P.A, Byrski T, Duchene G,

De France G, Hannachi F, Jones G.D, Kharraja B, *Calibration of new composite 'clover" detector as a Compton polarimeter for the Eurogamm array,* Nuclear Instruments and methods in Physics Research A 362 (1995) 556-560.

[JOS97] Joshi P.K, Jain H.C, Medhi, A.S, Chattopadhyay S, Bhattacharya S, Goswami A, *Study of the characteristics of a clover detector,* Nuclear Instruments and methods in Physics Research A 399 (1997) 51-56.

[KAL86] M. H. Kalos and P. A. Whitlock, *Monte Carlo Methods, Volume I: Basics*, Wiley-Interscience Publications, John Wiley and Sons, New York, 1986.

[KNO01] Knoll G.F, *Radiation detection and measurement*, Chapter 2-4 and 12, 2001, John Wiley and Sons, Inc.

[KRA88] Krane K.S, *Introductory nuclear physics,* pp 192-227, John Wiley and Sons, 1988.

[LAB00] Laborie J.M., Le Petit G., Abt D., Girarad M., Monte Carlo calculations of the efficiency calibration curve and coincidence – summing corrections in low – energy gamma – ray spectrometry using well – type HPGe detectors, Applied Radiation and Isotopes 53 (2000), pp. 57 – 62.

[LAW99] J. J. Lawrie, B. R. S. Babu, S. V. Förtsch, S.Naguleswaran, J. V. Pilcher, C. Rigollet, J. F. Sharpey-Schafer, F. D. Smit, C. J. Stevens, G. F. Steyn, and C. V. Wikner R. Beetge, G Mabala, D. Roux, and W. Whittaker, *Performance characteristics of the AFRODITE gamma-ray at NAC*, poster.

[LIL01] Liley J, *Nuclear Physics, Principles and Applications,* John Wiley and Sons, Ltd, 2001.

[LIP06] Lipoglavsek M, Likar M, Vencelj M, Vidmar T, Bark R.A, Guerorguieva E, Komati F, Lawrie J.J, Maliage S.M, Mullins S.M Murray S.H.T, Ramashidzha T.M, *Measuring high energy γ-rays with Clover detectors,* Nuclear Instruments and Methods in Physics Research A 557 (2006) 523-527.

[MAN05] MCNPX User's Manual 2.5.0, Radiation Safety information Computational Centre, Los Alamos Laboratory, Los Alamos, New Mexico, April 2005, Edited by Pelowitz D.B.

[MET49] Metropolis N, Ulam S, *The Monte Carlo Method,,*Journal of American Statistical Association, Vol. 44, No 247, September 1949, pp 335-341.

[MIC86] Michel C, Emling H, Grosse E, Azgui F, Grein H, Wollersheim H.J Gaardhoje J.J, Herskind B, *Monte Carlo simulation of complex germanium detector systems and Compton Suppression Spectrometers,* Nuclear Instruments and methods in Physics Research A 251 (1986) 119-133.

[MCK05] G. W. McKinney J. W. Durkee, J. S. Hendricks, M. R. James, D. B. Pelowitz, L. S. Waters, F. X. Gallmeier, *MCNPX 2.5.0 – New Features Demonstrated, MC 2005, Chattanooga, TN, April 17-21, 2005.*

[NEW98] Newman R.T, J. J. Lawrie, B. R. S. Babu, S. V. Förtsch, S.Naguleswaran, J. V. Pilcher, C. Rigollet, J. F. Sharpey-Schafer, F. D. Smit, C. J. Stevens, G. F. Steyn, C. V. Wikner R. Beetge, G Mabala, D. Roux, and W. Whittaker, N.J Ncapayi, *High-spin studies with the AFRODITE Array, Balkan Physics Letters, Special Issue, 182-190, 1998.*

References

[PUC07] V.F.E. Pucknell, The MIDAS Multi Instance Data Acquisition System at http://npg.dl.ac.uk/MIDAS, 9 June 2009.

[RAD95] D.C. Radford, *ESCL8R and LEVITSR: Software for interactive graphical analysis of HPGe coincidence data sets,* Nuclear Instruments and methods in Physics Research A 361 (1995) 297-305.

[SCA06] Scates W, Hartwell, J.K, Aryaeinejad R, McIIwain M.E, *Optimization studies of a Compton spectrometer using experimentally validated Monte Carlo simulations,* Nuclear Instruments and methods in Physics Research A 556 (2006) 498-504.

[SCH07] M.A. Schumaker,, G. Hackman, C.J. Pearson, C.E. Svensson, C. Andreoiu, A. Andreyev, R.A.E. Austin, G.C. Ball, D. Bandyopadhyay, A.J. Boston, R.S. Chakrawarthy, R. Churchman, T.E. Drake, P. Finlay, P.E. Garretta, G.F. Grinyer, B. Hyland, B. Jones, R. Maharaj, A.C. Morton, A.A. Phillips, F. Sarazin, H.C. Scraggs, M.B. Smith, J.J. Valiente-Dobo,1, J.C. Waddington, L.M. Watters, *Measured and simulated performance of Compton-suppressed TIGRESS HPGe clover detectors,* Nuclear Instruments and Methods in Physics Research A 570 (2007) 437–445.

[SHA88] Sharpey-Schafer J.F, Simpson J, *Escape Suppressed Spectrometer Arrays: A Revolution in γ-ray spectroscopy,* Progress in Particle and Nuclear Physics, 21, 1988, 293-399.

[SHA08] Sharpey-Schafer J.F**,** *Design of New Generation of High Sensitivity Gamma-ray Detectors,* Application for Research Funding as part of South African science and technology collaboration with the Russian Joint Institute for Nuclear Research (JINR), *April 2008.*

[SIM99] Simpson J, *The limits of gamma-ray spectroscopy with multi-detector arrays,* Nuclear Physics A654 (1999) 178c-194c.

[SIM09] Sima O, Arnold D, *On the Monte Carlo simulation of HPGE gamma-spectrometrysystems,* Applied Radiation and Isotopes 67 (2009), 701-705.

[VEN05] Venkataraman R, Croft S, Russ W.R, *Calculation of peak-to-total ratios for high purity germanium detectors using Monte Carlo modeling,* Journal of Radioanalytical and Nuclear Chemistry, Vol. 264, No 1, 2005, 183-191.

Appendix A

Material Compositions

Bismuth Germanate (BGO)

Density (g/cm^3) **7.13**

Nuclide	atomic fraction
Bi	4
Ge	3
O	12

Aluminum : Al

Density (g. cm^{-3}) **2.70**

nuclide	atomic fraction
Al	1

Hyper pure Germanium: Ge

Density (g. cm^{-3}) **5.32**

Nuclide	atomic fraction
Ge	1

Lanthinum Silicate-LSO

Density (g. cm^{-3}) **5.31**

Nuclide	atomic fraction
La	4
Si	3
O	12

Lead Tungstate-PbWO

Density (g. cm^{-3}) **8.31**

Nuclide	atomic fraction
Pb	1
W	1

O	4

Air

Density (g.cm^{-3})

nuclide	weight fraction
O	0.231781
N	0.755267
C	0.000125
Ar	0.012827

Tungsten-W

Density (g. cm^{-3})	**19.35**
Nuclide	atomic fraction
W	1

Appendix B

Typical MCNPX input file for suppression simulation

```
c Moddeling of a HPGe element ONLY (single Mode)
c  ============================================
c
c Cell Card
c ==========
c
1   1 -5.23     -3  2  6 -7  -10  IMP:P,E =1
2   1 -5.23     -5  2 -6  8  -10  IMP:P,E =1
3   1 -5.23     -4 -2 -6  8    9  IMP:P,E =1
4   1 -5.23     -1 -2  6 -7    9  IMP:P,E =1
c
6   4 -2.70       11 -12              IMP:P,E =1
$Cryostat can
c
24  4 -2.70       24 -25              IMP:P,E=1  $Cold
Aluminum can
c
11  0            -11 #1  #2 #3 #4          IMP:P,E=1
$Vacuum
c
7   2 -7.13       14 -13  16 -19 17 -18  IMP:P,E=1 $Right
BGO
8   2 -7.13       14 -13 -15  20 17 -18  IMP:P,E=1 $Right
BGO
9   2 -7.13       14 -13  20 -19 18 -21  IMP:P,E=1 $Top
BGO
10  2 -7.13       14 -13  20 -19 -17 22  IMP:P,E=1
$Bottom BGO
c
25  5 -19.35        13 -30  29 -28 -26 27  IMP:P,E=1 $Top
Col
26  5 -19.35        13 -30  29 -28 -32 33  IMP:P,E=1 $Bot
Col
27  5 -19.35       13 -30  34 -28 -27 32  IMP:P,E=1
$Right Col
28  5 -19.35       13 -30  29 -35 -27 32  IMP:P,E=1 $Left
Col
c
39  3  -1.20484e-3   -40  12 #7 #8 #9 #10 #11 #24 #25 #26
#27 #28  IMP:P,E =1 $Vacuum Around detector
40  0             40                              IMP:P,E
=0 $Outside world

c Surface Card
c =============
c
c Detector represented by a cylinder along the z axis
c ================================================
1  RCC    0  7.95 10  7 0 0  2.5     $ Top left dector
main body
```

```
2  PY     10                            $ Cut along Y
3  RCC    0 12.05 10  7 0 0  2.5       $ Top Right detector
main body
c
4  RCC    0 7.95  5.90 7 0 0 2.5       $Bottom Left
detector main body
5  RCC    0 12.05 5.90 7 0 0 2.5       $Bottom Right
detector main body
6  PZ     7.95                          $Cut along Z
c
7  P 7 5.45 12.05  7 14.55 12.05  3.6 5.45  12.5   $Top
incline
8  P 7 5.45  3.85  7 14.55  3.85  3.6 5.45  3.40
$Bottom Plane
9  P 7 5.90  12.5  7  5.90  3.40  3.6 5.45  12.5   $Left
Plane outcline
10 P 7 14.10 12.5  7  14.1  3.40  3.6 14.55 12.5   $Right
Outcline
c
11 RPP  -2.00  9.50   5.10   14.90      3.05   12.85
$Alliminium Can-HPge
12 RPP  -2.15  9.65   4.95   15.05      2.90   13.00
$Alliminium Can-HPge
c
24 RPP  -11.435  -2.15  5.10 14.90 3.05 12.85
25 RPP  -11.435  -2.15  4.60 15.40 2.55 13.35
c
13 PX      13       $Back Plane
14 PX   -11.2       $Front Plane
15 PY     4.6       $Left Plane
16 PY    15.4       $Right Plane
17 PZ    2.55       $Bottom Plane
18 PZ    13.5       $Top Plane
c
c Shield Planes
c ============
19 P -11.2  17.4  15.5    -11.2  17.4  0.55    13  15.8
13.9  $Right Plane
20 P -11.2   2.6  15.5    -11.2   2.6  0.55    13  4.2
13.9  $Left Plane
21 P -11.2   2.6  15.5    -11.2  17.4  15.55   13  4.2
13.9  $Top Plane
22 P -11.2   2.6  0.55    -11.2  17.4   0.55   13  4.2
2.15  $Bottom Plane
c
c Collimator Planes
c ================
c
26 P 13 15.8 13.9   13 4.2   13.9   16.55 4.763   13.337
$Top Top Col
27 P 13 4.2  12.05  13 15.8  12.05  16.55 4.763   11.487
$Top Bot Col
28 P 13 15.8 15.237 13 15.8 2.15   16.55 15.237  2.713
$Right Right Col
29 P 13 4.2  15.5   13 4.2  2.15   16.55 4.763   2.713
$Left Left Col
c
```

```
32 P 13 15.8 4     13  4.2    4     16.55 4.763   4.563
$Bottom Top
33 P 13 4.2  2.15  13  15.8  2.15   16.55 4.763   2.713
$Bottom Bottom
c
34 P 13 13.95 12.05  13 13.95 4.00   16.55 13.387 4.563
$Right Left
35 P 13 6.05  12.05  13 6.05  4.00   16.55  6.613 4.562
$Left Right
c
30 PX 16.55
c
40 RPP -15  40  -15 40  -15 40

c Data Cards
c ===========
Mode P E
c
m1    32000      1                    $ HPGe
c
c Shield Material-BGO
m2     83000      4 &                 $Bismuth
       32000      3 &                 $Germanium
        8000      12                  $Oxide
c Air
m3    8000     -0.231781 &           $Oxygen
      7000     -0.755267 &           $Nitrogen
      6000     -0.000125 &           $Carbon
      18000    -0.012827             $Argon
c
c Alliminium
m4 13000 1
c
c Tungstate
m5 74000 1
c
c Source definition
c =================
c Isotropic point source
SDEF PAR P POS 26.5 10 7.95 VEC -1 0 0 DIR D1 ERG D2
SI1 -1 0.9965 1
SP1 0 0.95 0.05
SI2 L 1.173 1.332
SP2   0.999 1.000
c
c
f26:e  (2 3 4 7 8 9 10)   $ BGO energy dep.
ft26   GEB 0 0.001834 0
sd26   1
f36:e  1                  $ HPGe energy dep.
ft36   GEB 0 0.001834 0
sd36   1
f18:e  1                  $ BGO/HPGe PHT
e18    0. 1.173  1.332
fu18   0. 2799i 1.400
ft18   phl 1 26 1 1 36 1
fq18   u e
c
```

```
c
c
ctme   2880            $ 2880 minutes
PRINT
```